ORIGINAL RESEARCH

Caveolae-Mediated Activation of Mechanosensitive Chloride Channels in Pulmonary Veins Triggers Atrial Arrhythmogenesis

Yuriy V. Egorov, PhD;* Di Lang, PhD;* Leonid Tyan, PhD; Daniel Turner, BS; Evi Lim, BS; Zachary D. Piro, BS; Jonathan J. Hernandez, PhD; Rylie Lodin, BS; Rose Wang, BS; Eric G. Schmuck, PhD; Amish N. Raval, MD; Carter J. Ralphe, MD; Timothy J. Kamp, MD, PhD; Leonid V. Rosenshtraukh, DSc, PhD; Alexey V. Glukhov, PhD

***Background*—**Atrial fibrillation often occurs in the setting of hypertension and associated atrial dilation with pathologically increased cardiomyocyte stretch. In the setting of atrial dilation, mechanoelectric feedback has been linked to the development of ectopic beats that trigger paroxysmal atrial fibrillation mainly originating from pulmonary veins (PVs). However, the precise mechanisms remain poorly understood.

***Methods and Results*—**We identify mechanosensitive, swelling-activated chloride ion channels ($I_{Cl,swell}$) as a crucial component of the caveolar mechanosensitive complex in rat and human cardiomyocytes. In vitro optical mapping of rat PV, single rat PV, and human cardiomyocyte patch clamp studies showed that stretch-induced activation of $I_{Cl,swell}$ leads to membrane depolarization and decreased action potential amplitude, which trigger conduction discontinuities and both ectopic and reentrant activities within the PV. Reverse transcription quantitative polymerase chain reaction, immunofluorescence, and coimmunoprecipitation studies showed that $I_{Cl,swell}$ likely consists of at least 2 components produced by mechanosensitive ClC-3 (chloride channel-3) and SWELL1 (also known as LRRC8A [leucine rich repeat containing protein 8A]) chloride channels, which form a macromolecular complex with caveolar scaffolding protein Cav3 (caveolin 3). Downregulation of Cav3 protein expression and disruption of caveolae structures during chronic hypertension in spontaneously hypertensive rats facilitates activation of $I_{Cl,swell}$ and increases PV sensitivity to stretch 10- to 50-fold, promoting the development of atrial fibrillation.

***Conclusions*—**Our findings identify caveolae-mediated activation of mechanosensitive $I_{Cl,swell}$ as a critical cause of PV ectopic beats that can initiate atrial arrhythmias including atrial fibrillation. This mechanism is exacerbated in the setting of chronically elevated blood pressures. **(*J Am Heart Assoc*. 2019;8:e012748. DOI: 10.1161/JAHA.119.012748.)**

Key Words: arrhythmia • caveolae • caveolin 3 • hypertension • mechanoelectrical transduction • pulmonary veins • stretch • volume-activated chloride channels

Atrial fibrillation (AF) is the most common cardiac rhythm disorder and is often associated with hypertension, heart failure, and valvular heart disease.[1,2] These conditions cause hemodynamic pressure and volume overload of the atria, resulting in stretching of the atrial cardiomyocytes. Though AF maintenance is most likely a reentrant phenomenon conditioned by elevated electrophysiological and/or structural heterogeneity, the precise pathophysiological basis for triggers that initiate AF has not been resolved. Regions within the atria around the pulmonary vein (PV) ostia are subject to the most significant dilation and are known to be the most common regions to develop arrythmogenic ectopic foci.[3] The PVs are often responsible for AF initiation in patients and thus are commonly targeted during catheter or surgical AF ablation procedures, which cure 75% of paroxysmal AF cases.[4,5] Animal and human studies demonstrate that acute stretch facilitates PV arrhythmogenesis by increasing dispersion of refractoriness, leading to heterogeneous intra-

From the Laboratory of Heart Electrophysiology, Cardiology Research Centre, Moscow, Russian Federation (Y.V.E., L.V.R.); Department of Medicine, Cardiovascular Medicine (D.L., L.T., D.T., E.L., Z.D.P., J.J.H., R.L., R.W., E.G.S., A.N.R., T.J.K., A.V.G.) and Department of Pediatrics, Pediatric Cardiology (J.J.H., C.J.R.), University of Wisconsin-Madison School of Medicine and Public Health, Madison, WI.

Accompanying Data S1, Table S1, and Figures S1 through S10 are available at https://www.ahajournals.org/doi/suppl/10.1161/JAHA.119.012748

*Dr Egorov and Dr Lang contributed equally to this work.

Correspondence to: Alexey V. Glukhov, PhD, 8455 WIMR II, 1111 Highland Ave., Madison, WI 53705. E-mail: aglukhov@medicine.wisc.edu

Received July 16, 2019; accepted September 13, 2019.

© 2019 The Authors. Published on behalf of the American Heart Association, Inc., by Wiley. This is an open access article under the terms of the Creative Commons Attribution-NonCommercial License, which permits use, distribution and reproduction in any medium, provided the original work is properly cited and is not used for commercial purposes.

Clinical Perspective

What Is New?

- We link specialized cardiac cell membrane structures, caveolae, to the activation of mechanosensitive chloride ion channels and the development of arrhythmogenic ectopic beats from pulmonary veins, the most common source of paroxysmal atrial fibrillation.
- Downregulation of caveolae structures during chronic hemodynamic overload of the atria facilitates activation of chloride ion channels and increases sensitivity of pulmonary veins to stretch.

What Are the Clinical Implications?

- Our study provides conceptual innovation on cardiac mechanosensing, which critically contributes to atrial arrhythmogenesis associated with elevated blood pressure, atrial dilation, and pathologically increased cardiomyocyte stretch.
- It forms a mechanistic basis for development of novel and effective therapeutic approaches targeted to treat stretch-induced atrial arrhythmogenesis by preventing the degradation or promoting the restoration of cardiac cytoarchitecture.

PV conduction slowing and triggered automaticity inside the PV.[6,7] Based on the relationship between stretch and arrhythmogenesis, mechanoelectric feedback has been proposed as the principal mediator of the disease,[8,9] although the precise mechanisms remain poorly understood.

Specialized surface membrane structures, referred to as *caveolae*, represent small (50- to 100-nm) invaginations of the plasma membrane and are enriched by cholesterol, sphingolipids, and scaffolding proteins called *caveolins*.[10,11] Caveolae represent a reserve source of "extra" cell membrane and are implicated in mechanotransduction by buffering mechanical forces and contributing to cell volume regulation.[10] It is estimated that, in the rat ventricular myocyte, 22% of the cell membrane resides in caveolae[12] and that stretch of the cell incorporates this reserved membrane into the surface membrane via flattening of caveolae.[10,11]

In addition to their ability to influence cell volume, it has been shown in various cell types that caveolae are involved in mechanoelectrical transduction,[13,14] possibly by promoting the activation of mechanosensitive ion channels, including swelling-activated chloride ion (Cl^-) channels ($I_{Cl,swell}$).[10] The presence of $I_{Cl,swell}$ has been shown in myocytes isolated from rabbit PVs.[9] In guinea pig ventricular myocytes, activation of $I_{Cl,swell}$ depolarizes the membrane resting potential (RP),[15] which may slow electrical impulse conduction. In Langendorff-perfused isolated mouse hearts, pressure loading significantly decreases the ventricular conduction velocity, along with a concomitant decrease in caveolae density, both of which are restored on pressure unloading.[11] Pathological conditions associated with elevated chronic stretch, including AF, hypertension, and hypertrophy, are linked to a decrease in cardiomyocyte caveolae density and downregulation of the muscle-specific caveolae scaffolding protein Cav3 (caveolin 3).[16–18] These findings suggest a crucial role of caveolae and caveolar ion channels in stretch-induced electrophysiological changes facilitating PV arrhythmogenesis.

In this study, we show that volume-activated Cl^- channels $I_{Cl,swell}$ are localized in the caveolae microdomains and can be activated on mechanical stretch. $I_{Cl,swell}$ likely consists of at least 2 components produced by mechanosensitive ClC-3 (chloride channel-3) and SWELL1 (also known as LRRC8A [leucine rich repeat containing protein 8A]) channels that form a mechanosensitive macromolecular complex with caveolar scaffolding protein Cav3. Activation of $I_{Cl,swell}$ results in an inward current in the distal part of the PV (PV_{dis}). This, in turns, leads to tension-dependent depolarization of the membrane RP suppressing action potential (AP) amplitude (APA) and resulting in intra-PV conduction discontinuities as well as ectopic and reentrant activities within the PV. Downregulation of Cav3 expression and disruption of caveolae structures during hypertension facilitates activation of $I_{Cl,swell}$ and increases sensitivity to stretch 5- to 10-fold, promoting the development of AF. Our findings identify caveolae-mediated activation of mechanosensitive $I_{Cl,swell}$ as a critical cause of the triggering impulses that can initiate atrial arrhythmias including AF, and this mechanism is exacerbated in the setting of chronically elevated blood pressures (BPs). These findings identify new therapeutic targets for atrial arrhythmias.

Methods

A detailed materials and methods section is found in Data S1. The data that support the findings of this study are available from the corresponding author on reasonable request.

Animals and Preparations

All methods and protocols used in these studies were approved by the animal care and use committee of the Cardiology Research Center (Moscow, Russia) and the University of Wisconsin–Madison following the *Guidelines for Care and Use of Laboratory Animals* published by the National Institutes of Health (NIH; publication no. 85-23, revised 1996). All animals used in this study received humane care in compliance with the *Guide for the Care and Use of Laboratory Animals*. Human heart collection protocols were approved by the University of Wisconsin institutional review board.

Adult (8–12-month-old) normotensive Wistar rats (n=62) and spontaneously hypertensive rats (SHRs; n=17) of both sexes were used. The PV preparations were isolated as previously described.[19] Briefly, the left atrium (LA), together with the LA appendage and PV region, was dissected from the ventricles, right atrium, and interatrial septum. The central PV was cleaned, cut open, and placed in a tissue bath with the endocardial side facing upward (Figure 1A). The pacing electrode was placed on the edge of the LA appendage. A small portion of the end-distal part of the PV was not cut open and was used to weave a silk suture (4-0) with a weight applied (Figure 1A).

Microelectrode Recordings

Transmembrane APs were simultaneously recorded from the endocardial surface of the proximal (PV ostium [PV_{ost}]) and PV_{dis} preparations by using 2 glass microelectrodes filled with 3.0 mol/L KCl (tip resistance ≈15–40 MΩ).[19]

Optical Mapping

PV preparations were stained with voltage-sensitive dye RH237 (10 μmol/L; Thermo Fisher Scientific) and optically mapped with a MiCAM Ultima-L CMOS camera (SciMedia USA) from the endocardial field of view ranging from 10×10 to 16×16 mm^2, sampled at 1000 to 3000 frames/s.[20]

Patch Clamp Studies

Patch clamp measurements of $I_{Cl,swell}$ current and spontaneous electrical activity were performed on cardiomyocytes isolated from PV_{dis} and PV_{ost}, and on human induced pluripotent stem cell–derived cardiomyocytes (hiPS-CMs) generated from the well-characterized DF19-9-11T line.[21]

Immunohistochemistry

Masson's trichrome staining and double-immunolabeling for ClC-2 (goat polyclonal; SAB2501373, Sigma-Aldrich), ClC-3 (rabbit polyclonal; ACL-001, Alomone Labs), SWELL1 (anti-LRRC8A, rabbit polyclonal; AAC-001, Alomone Labs), and Cav3 (mouse monoclonal; 610421, BD Biosciences; rabbit polyclonal; ab2912, Abcam) were performed on paraffin-embedded sections of unstretched PV preparations. Images were collected using a Leica SP5 confocal microscope system under ×63 oil-immersion objective and analyzed using the NIH ImageJ and Matlab software.

Immunoprecipitation

Rat PV and healthy human LA tissue lysates were used, and immunoprecipitations were carried out using anti-Cav3 or anti–ClC-2, anti–ClC-3, or anti-SWELL1 antibodies; control IgGs (respective to sample species) were used at the same concentrations as the specific antibodies. Immune complexes were analyzed by Western blot by probing with antibodies specific for ClC-2, ClC-3, SWELL1, Cav3, and GAPDH.

Quantitative Reverse Transcription Polymerase Chain Reaction Analysis

Total RNA was extracted from rat PV_{dis}, PV_{ost}, and LA using TriZol reagent (Invitrogen). Quantitative reverse transcription polymerase chain reaction for *ClC-2*, *ClC-3*, *LRRC8A*, *ANO1* (anoctamin 1), *Cav3*, and *GAPDH* (probes are listed in Table S1) were performed using TaqMan Fast Advanced Master Mix (Thermo Fisher Scientific). Levels of mRNA were quantified using the ΔΔCt method and normalized to housekeeping gene *GAPDH*.

Statistical Analysis

Student *t* test was used in 2-group comparisons (paired for comparisons between the same participant and unpaired for 2 groups of different participants). Multiple groups of normally distributed data of similar variance were compared by 1- or 2-way ANOVA (for nonrepeated measurements) or repeated-measurements 2-way ANOVA. For multiple comparisons, the Bonferroni corrected *P* value is shown. All statistical analyses were performed using GraphPad Prism 5 (GraphPad Software) or Origin v6.1 (OriginLab). $P<0.05$ was considered statistically significant. Values were presented as mean±SEM.

Results

Electrophysiological Changes in the PV Under Stretch

We modeled the effect of physiological and pathological stretch on Wistar rat PV preparations by applying weights across 2 ranges: 0 to 1.5 g of weight corresponding to a physiological pulmonary venous pressure range from 0 to ≈4 mm Hg (calculated as applied weight times gravity constant divided by cross-section area of the PV preparation) and 2.5 to 10.5 g of weight corresponding to a pathological pressure range from ≈6 to 26 mm Hg. We used simultaneous microelectrode recordings of transmembrane AP from PV_{dis} (near the lung) and PV_{ost} (near the LA) to measure PV response to stretch (Figure 1A). Physiological stretch induced a heterogeneous prolongation of both AP duration and functional refractory period along the PV, with no effect on RP and APA (Figures S1 through S3). It resulted in a significant increase in the dispersion of refractoriness along the PV (from 3±2 ms at baseline up to 26±5 ms at 1.5 g;

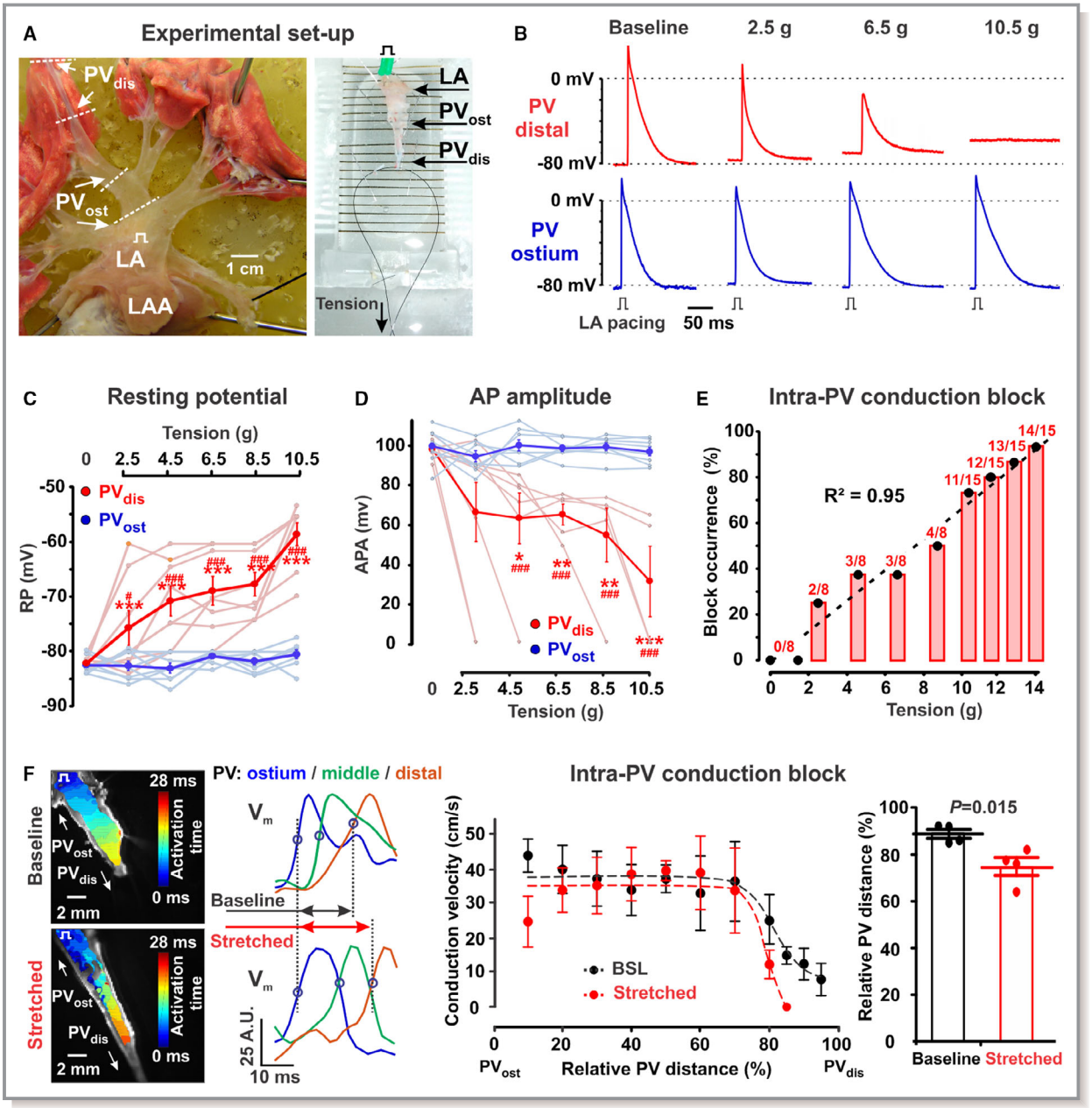

Figure 1. Effect of pathological stretch on the pulmonary vein (PV) myocardium. **A**, Photograph of the intact rat PVs (left). Central PV was isolated, cleaned, cut open, and placed in a tissue bath with the endocardial side facing upward (right). Anatomical regions selected for microelectrode action potential (AP) recordings are shown: PV ostium (PV_{ost}) and PV distal (PV_{dis}). **B**, Representative examples of APs simultaneously recorded in the PV_{dis} (top recordings) and PV_{ost} (bottom recordings) under different pathological stretch. **C** and **D**, Membrane resting potential (RP) and AP amplitude (APA) changes for individual rats (light blue lines indicate PV_{ost}, and red lines indicate PV_{dis}) and averaged (solid lines). **E**, Probability (in percentage from total preparations tested) of intra-PV conduction block at different tensions. Data include 2 series of experiments: n=8 for tensions <10.5 g, and n=15 for tensions >10.5 g. **P*<0.05, **<0.01, ***<0.001 within the same group vs baseline, and $^{\#}P$<0.05, $^{\#\#\#}$<0.001 for PV_{dis} vs PV_{ost} by repeated-measurements 2-way ANOVA with Bonferroni correction. **F**, Fluorescent optical mapping of electrical activity during the development of intra-PV conduction block under pathological stretch. At left, PV activation maps are shown at baseline (no stretch applied; top) and during the development of intra-PV conduction block (stretched; bottom). In the middle, superimposed upstrokes of optical action potentials (V_m) along the PV (PV_{ost} in blue, PV middle in green, and PV_{dis} in red) are shown for each condition. At right, distribution of conduction velocity along the PV and relative PV distance (in percentage from the PV length from a brightfield image) activated at baseline and during stretch. *P* value was determined by paired Student *t* test. **G** and **H**, Microreentry within the PV occurred under pathological stretch and application of norepinephrine (1 μmol/L). LA indicates left atrium; LAA, left atrial appendage.

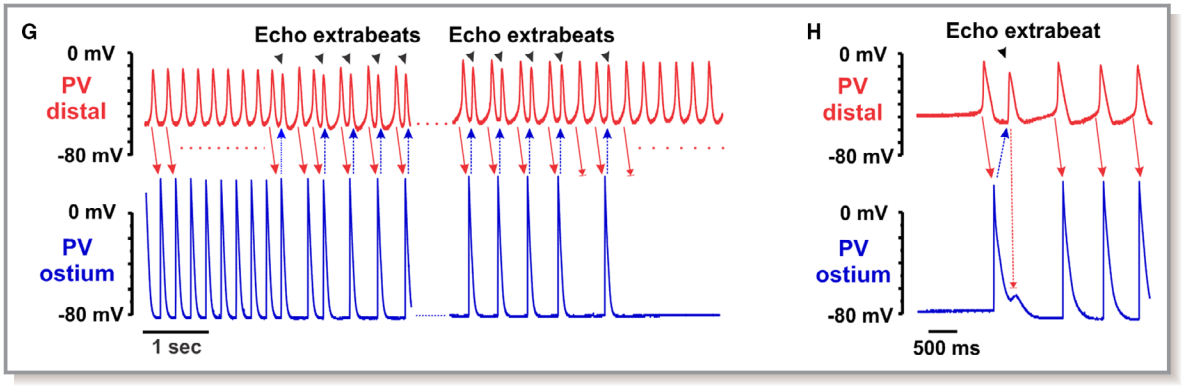

Figure 1. Continued

$P<0.01$) and the development of spontaneous activity as well as the induction of early after-depolarizations in the PV_{dis} (Figure S1).

In contrast to physiological stretch, pathological stretch induced dramatic changes in RP and APA exclusively in the PV_{dis} and was accompanied by the subsequent development of intra-PV conduction block (Figure 1B–1D), correlating with the degree of tension applied (Figure 1E). Consistent with our microelectrode measurements, high-resolution fluorescent optical mapping of electrical activity revealed intra-PV conduction block in all Wistar rats (n=4) under pathological stretch (Figure 1F). Conduction velocity slowing and conduction block were found distally in the PV (at ≈60–80% of the PV length), which is consistent with previous studies in both canine[22] and human PVs.[7] As seen from optical mapping images, pathological stretch that was required to induce intra-PV conduction block and led to ≈30% to 40% lengthening of the PV tissue. Importantly, tension was applied homogeneously along the PV, as estimated from the cardiomyocyte sarcomere length measured from immunofluorescent images for α-actinin staining (for maximal tension, sarcomere length increased from 1.19±0.03 μm to 1.74±0.05 in PV_{ost} and from 1.20±0.04 to 1.65±0.06 μm in PV_{dis}, not significant between regions; Figure S4).

Reentrant Arrhythmias Induced by Stretch in the PVs

Application of 1 μmol/L norepinephrine always triggered spontaneous automaticity from the PVs. However, at depolarized RP during pathological stretch, norepinephrine led to more regular and faster PV automaticity compared with baseline (the fastest spontaneous beating rate was 118±28 beats/min at 6.2±1.5 g versus 50±13 beats/min at baseline; $P=0.049$; Figure S5). In some preparations (2/8 at 0.1 g, 1/8 at 2.5 g, 1/8 at 4.5 g, 2/8 at 6.5 g, 2/8 at 8.5 g, and 1/8 at 10.5 g), norepinephrine-induced paroxysms of spontaneous activity were associated with echo beats (Figure 1G and 1H; Figure S6). In the example shown in Figure 1G, spontaneous AP generated in the PV_{dis} during norepinephrine perfusion with 4.5-g tension (top recording) propagated to the PV_{ost} (bottom recording) and induced an AP that subsequently reexcited the PV_{dis} and led to the echo *extrabeat* (note the shorter coupling interval between the echo extrabeat and the previous spontaneous AP as well as the different extrabeat AP morphology). Another example shows one and a half reentry circle captured in the PV preparation under 6.5-g tension and norepinephrine perfusion (Figure 1H). The echo extrabeat from the PV_{dis} reexcited the PV_{ost} and induced a nonpropagating response.

Impact of Volume-Activated Cl^- Channels on Stretch-Induced PV Arrhythmogenesis

To ascertain the impact of mechanosensitive Cl^- channels on stretch-induced changes in PV electrophysiology, we tested $I_{Cl,swell}$ inhibitors on the intra-PV conduction block. First, the applied tension was adjusted to induce PV RP depolarization and conduction block (characterized by RP above −60 mV and APA <20 mV). The tensions varied from 10.5 g (75% probability of conduction block) to 13.5 g (94%; Figure 1E). Application of nonselective inhibition of $I_{Cl,swell}$ by DIDS (4,4′-diisothiocyanato-2,2′-stilbenedisulfonic acid disodium salt; 100 μmol/L, n=7) restored conduction in all preparations tested, significantly ($P<0.001$) hyperpolarizing the RP and increasing the APA (Figure 2A). Similarly, selective inhibition of $I_{Cl,swell}$ by DCPIB (4-[(2-butyl-6,7-dichloro-2-cyclopentyl-2,3-dihydro-1-oxo-1H-inden-5-yl)oxy]butanoic acid; 100 μmol/L, n=9) quickly (<5 minutes) hyperpolarized the RP and restored conduction in the PV_{dis} (Figure 2B). Washout of DCPIB abolished its effects, and conduction block returned.

To test whether calcium-activated Cl^- channel ANO1 (anoctamin 1; also known as TMEM16A [transmembrane member 16A]), which might be activated by a possible intracellular [Ca^{2+}] elevation on stretch, contributes to the observed stretch-induced intra-PV conduction dissociation,

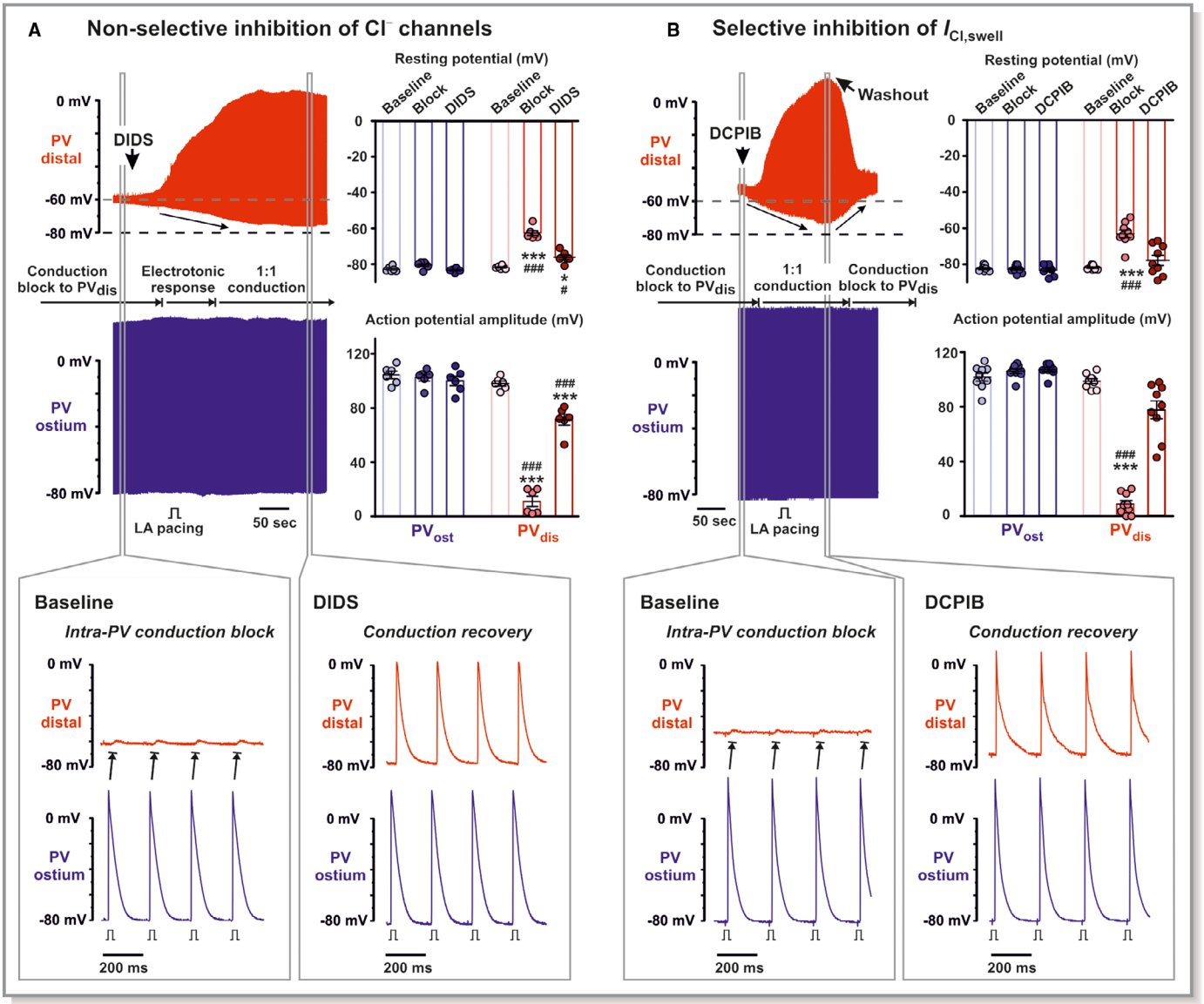

Figure 2. Inhibition of volume-activated chloride ion (Cl^-) channels hyperpolarizes resting potential (RP) in pulmonary veins distal (PV_{dis}) and restores intra-PV conduction in stretched PVs. Two simultaneous microelectrode recordings from PV_{dis} (top recording in red) and PV ostium (PV_{ost}; bottom recording in blue) are shown during conduction block and after application of nonselective chloride current blocker DIDS (**A**) or selective swelling-activated chloride ion channel ($I_{Cl,swell}$) blocker DCPIB (**B**) (shown by arrows). Selected time windows (gray rectangles) are shown enlarged in corresponding panels. Left atrium (LA) was constantly paced with S1S1=300 ms. Notice progressive hyperpolarization of RP (shown by arrows) during conduction recovery. Transmembrane potential levels of −60 and −80 mV are shown by dotted lines for PV_{dis} recording. At right, action potential amplitude and RP are shown at baseline (no stretch applied), during intra-PV block (Block) and after application of corresponding $I_{Cl,swell}$ antagonists. n=7 for DIDS and n=9 for DCPIB. $^*P<0.05$, $^{***}<0.001$ vs baseline, and $^{\#}P<0.05$, $^{\#\#\#}<0.001$ for PV_{dis} vs PV_{ost} by repeated-measurements 2-way ANOVA with Bonferroni correction. DCPIB indicates 4-[(2-butyl-6,7-dichloro-2-cyclopentyl-2,3-dihydro-1-oxo-1H-inden-5-yl)oxy]butanoic acid; DIDS, 4,4′-diisothiocyanato-2,2′-stilbenedisulfonic acid disodium salt.

we applied the ANO1-selective inhibitor NPPB (5-nitro-2-[3-phenylpropylamino] benzoic acid ; 10 μmol/L) and found no effect on either PV_{dis} RP or intra-PV conduction block within 30 minutes of treatment (data not shown).

To correlate the observed effects with the underlying activation of $I_{Cl,swell}$, cardiomyocytes were enzymatically isolated separately from the rat PV_{dis} and PV_{ost}. $I_{Cl,swell}$ was activated by osmotic swelling from relative osmolality of 1T to 0.7T (Figure 3A). Patch clamp studies revealed swelling-activated, DCPIB-sensitive Cl^- current specifically in PV_{dis} but not in PV_{ost} cardiomyocytes; this finding correlates well with the electrophysiological effects of stretch observed on the intact PV (Figures 1 and 2). These results are in agreement with a functional presence of DIDS-sensitive chloride current shown in isolated rabbit PV myocytes in response to both axial cell stretch and hypotonic cell swelling.[9]

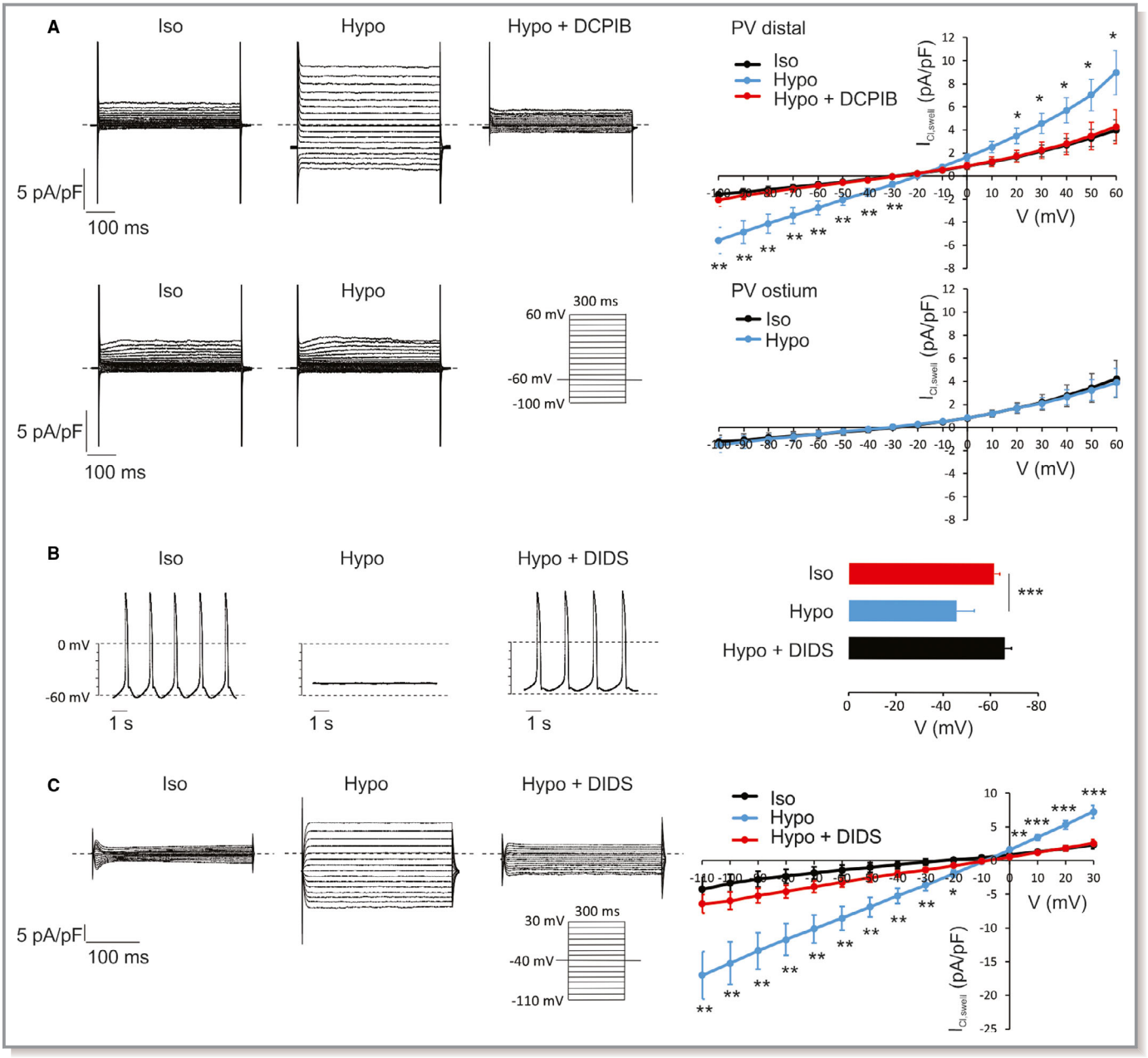

Figure 3. Activation of swelling-activated chloride ion channels ($I_{Cl,swell}$) leads to resting potential depolarization and inhibition of spontaneous electrical activity in single cardiomyocytes. **A**, (Left) Whole-cell $I_{Cl,swell}$ recorded from single myocytes separately isolated from the pulmonary veins distal (PV_{dis}; n=8 for isotonic [Iso], n=8 for hypotonic [Hypo], and n=6 for Hypo plus DCPIB 10 μmol/L; upper panel) and PV ostium (PV_{ost}; n=4 for Iso and Hypo; lower panel), respectively, under Iso and Hypo conditions. DCPIB-sensitive activation of $I_{Cl,swell}$ was observed during Hypo condition exclusively in PV_{dis} myocytes. (Right) Corresponding current-voltage (I-V) curves for $I_{Cl,swell}$ from PV_{dis} (upper panel) and PV_{ost} (lower panel) myocytes. **B**, Activation of $I_{Cl,swell}$ current by Hypo cell swelling led to depolarization of the membrane resting potential (RP) and inhibition of spontaneous electrical activity in single human induced pluripotent stem cell-derived cardiomyocytes (iPS-CMs). DIDS (100 μmol/L) recovered the automaticity and RPs in the single iPS myocytes. ***P<0.001 vs Iso condition by 1-way ANOVA with Bonferroni correction. **C**, Similar to PV_{dis} myocytes, the effect was observed in single human iPS-CMs. *P<0.05, **0.01, ***0.001 vs treatment by 1-way ANOVA with Bonferroni correction. DCPIB indicates 4-[(2-butyl-6,7-dichloro-2-cyclopentyl-2,3-dihydro-1-oxo-1H-inden-5-yl)oxy]butanoic acid; DIDS, 4,4′-diisothiocyanato-2,2′-stilbenedisulfonic acid disodium salt.

To determine whether our findings apply to human cardiomyocytes, we used hiPS-CMs and modeled cellular stretch by osmotic swelling (Figure 3B and 3C).[9,23] Prior electrophysiology studies indicated that iPS cells have a capacity for differentiation into nodal-, atrial-, and ventricular-like phenotypes based on AP characteristics.[21] However, no

protocols are currently available to specifically differentiate iPS cells to PV cardiomyocytes or to isolate such a population of cells, so we chose experimental conditions in which most of the hiPS-CMs exhibited immature ventricular-like APs characterized by stable spontaneous activity and slightly depolarized maximum diastolic potential (−65±3 mV) similar to what was recorded previously from isolated canine PV myocytes (−66±1 mV in PV versus −74±1 mV in LA; $P<0.001$).[24] Activation of $I_{Cl,swell}$ current by hypotonic cell swelling led to depolarization of the membrane RP and inhibition of spontaneous electrical activity in a single hiPS-CM (Figure 3B). Similar to tissue level changes (Figure 2), inhibition of $I_{Cl,swell}$ by 100 μmol/L DIDS in the setting of hypotonic swelling hyperpolarized RP to baseline values and restored the spontaneous activity in hiPS-CMs. In addition, whole-cell patch clamp studies of hiPS-CMs demonstrated a DIDS-sensitive, swelling-activated Cl^- current (Figure 3C). These findings are consistent with human cardiomyocytes exhibiting electrophysiology similar to that observed in the rat PV cardiomyocytes.

Caveolar Mechanosensitive Complex

$I_{Cl,swell}$ current has been linked to the activation of ClC-2,[25] ClC-3,[26] and SWELL1[27] isoforms of sarcolemmal mechanosensitive Cl^- channels. Various studies associated mechanosensitive I_{Cl} with caveolae structures[10,13,28] in which these channels can be associated with the caveolar scaffolding proteins caveolins.[29] Our immunohistochemical analysis showed that ClC-2, ClC-3, and SWELL1 are all highly colocalized with myocyte-specific caveolar scaffolding protein Cav3 in both rat PV and human left atrial myocardium (Figure 4; negative controls are shown in Figure S7). Immunoprecipitation performed on rat PV myocardial lysate revealed that only ClC-3 and SWELL1, but not ClC-2, are associated with Cav3 (Figure 5). In contrast, both ClC-3 and ClC-2 are found to be associated with Cav3 in human left atrium (Figure S8), suggesting species dependence. Our comparative quantitative reverse transcription polymerase chain reaction analysis demonstrated that SWELL1 and ClC-3 channels demonstrate an equal abundance in both PV and LA myocardium, whereas ClC-2 channels (as well as calcium-activated Cl^- channel ANO1) show a 10-fold lower mRNA expression level compared with SWELL1 and ClC-3 channels.

Western blot analysis did not reveal any difference in the protein expression level for ClC-2, ClC-3, and SWELL1 along the PV, whereas the Cav3 expression level was higher in PV_{dis} versus PV_{ost} (Figure 6). This may indicate higher membrane reserve and thus more substantial $I_{Cl,swell}$ activation on stretch in PV_{dis} than in PV_{ost}, as it was observed in both the intact vein (Figures 1 and 2) and isolated PV cells (Figure 3). Together with a significantly lower expression level of the RP stabilizing inwardly rectifying K^+ current (I_{K1}) protein in the PV (Figure 6A and 6B; as also demonstrated previously[30]), these results may provide an explanation for the observed higher sensitivity of the PV_{dis} to caveolae-mediated stretch-induced depolarizing Cl^- current.

Hypersensitivity of SHR PVs to Stretch

Hypertension is one of the main risk factors of AF.[1] Clinical studies show that an acute increase in atrial pressure and sustained atrial dilatation can result in the development of AF.[2] Several studies using SHRs show increased incidence of AF and atrial tachyarrhythmias compared with normotensive rats.[31] In this study, we applied stretch protocols to SHR PV preparations (echo data indicating diastolic dysfunction and progress toward cardiac hypertrophy in SHRs are shown in Figure S9) and found that the tension required to induce intra-PV conduction block in SHRs is inversely correlated with the rat's BP (measured using tail cuff from lightly anesthetized rats). SHRs with BP >200 mm Hg (average BP of 219±6 mm Hg, average tension to induce conduction block was 0.30±0.03 g, n=3) developed conduction block at much smaller tensions, even within the physiological range, compared with SHRs with BP <200 mm Hg (average BP of 163±10 mm Hg, average tension to induce block was 1.6±0.7 g, n=3, $P<0.01$; Figure 7A, top). Both groups, however, had much higher sensitivity to developing intra-PV conduction block than Wistar rats (Figure 7A, bottom). In comparison to Wistar rats, SHRs showed significantly smaller APA in both PV_{ost} and PV_{dis}, mild RP depolarization, and a significantly prolonged functional refractory period (Figure S10), which may indicate the presence of constitutively active $I_{Cl,swell}$ that has been previously reported in both failing canine ventricular myocytes[23] and human atrial myocytes obtained from patients with right atrial enlargement and/or elevated left ventricular end-diastolic pressure.[32]

Optical mapping of electrical activity revealed a more pronounced intra-PV conduction dissociation in SHRs, with conduction block occurring more proximally to the PV_{ost} than in Wistar rats (Figure 7B). Similar to Wistar rats, inhibition of $I_{Cl,swell}$ by 9AC (9-anthracenecarboxylic acid; 100 μmol/L) recovered the AP propagation toward the PV_{dis}, confirming the contribution of mechanosensitive $I_{Cl,swell}$ in the stretch-induced intra-PV conduction dissociation.

For detailed analysis of PV mechanosensitivity associated with varied severity of hypertension, we separated SHRs into 2 groups with BP ≥200 and <200 mm Hg, respectively. SHRs with BP <200 mm Hg had significantly shorter and stretch-insensitive AP duration and functional refractory period compared with SHRs with BP >200 mm Hg (Figure 7C and 7D). In SHRs with BP <200 mm Hg, PV_{dis} was more sensitive

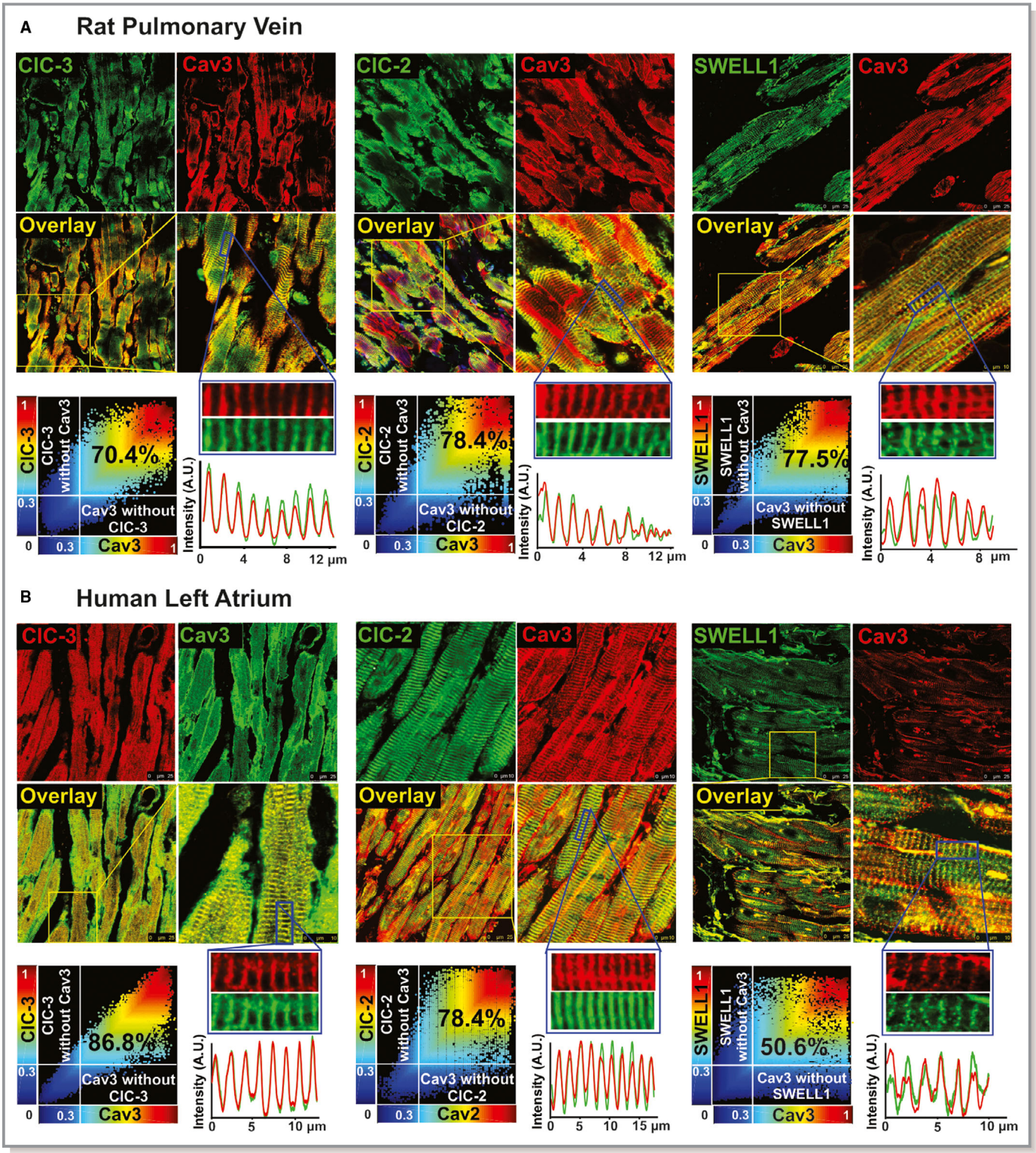

Figure 4. Caveolar macromolecular mechanosensitive complex. Immunofluorescent analysis of colocalized expression of ClC-3 (left), ClC-2 (middle), and SWELL1 (right) chloride channels with caveolae scaffolding protein Cav3 (caveolin 3) in nonstretched rat pulmonary vein distal (PV_{dis}; **A**) and human left atrium (**B**) myocardium. For colocalization analysis, intensity level of 30% was used as a threshold. Cav3 indicates caveolin 3; ClC, chloride channel; SWELL1, also known as LRRC8A (leucine rich repeat containing protein 8A).

to stretch than PV_{ost}, which was similar to that observed in Wistar rats (Figure 7E and 7F). In SHRs with BP >200 mm Hg, the entire PV was highly sensitive to stretch-induced changes in RP and APA, indicating more profound remodeling occurring along the PV in rats with severe hypertension versus either mild hypertension or normotension.

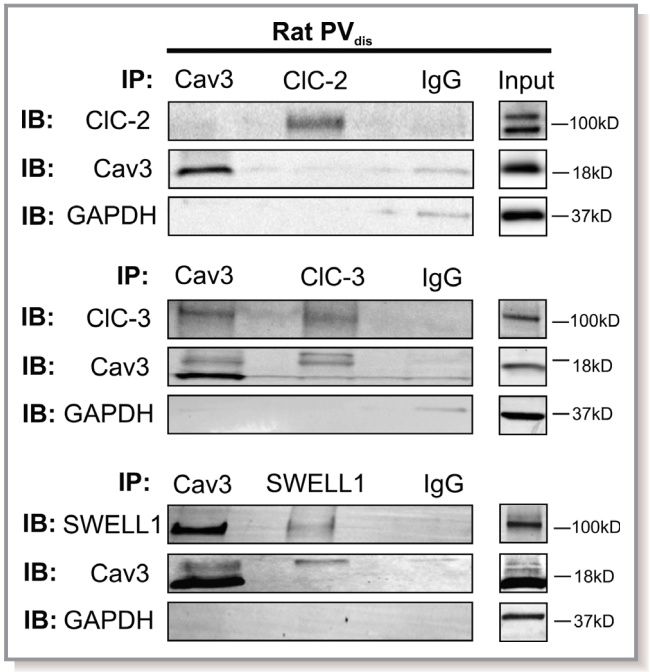

Figure 5. Co-IP Western blots showing degree of association of Cav3 and chloride channels ClC-2, ClC-3, and SWELL1 in rat pulmonary vein (PV; n=2). IB indicates immunoblot; IP, immunoprecipitation. Cav3 indicates caveolin 3; ClC, chloride channel; SWELL1, also known as LRRC8A (leucine rich repeat containing protein 8A).

Stretch-Induced Conduction Abnormalities Are Associated With Downregulation of Cav3

To determine whether hypersensitivity of SHR PV is associated with changes in ClC expression profile, we measured ClC-2, ClC-3, and SWELL1 protein expression and found no significant changes in levels in SHRs (Figure 8A). In contrast, SHRs demonstrated significant downregulation of Cav3 protein expression level compared with Wistar rats (Figure 8A). Downregulation of Cav3 was associated with a prominent decrease in caveolae density in SHRs assessed by transmission electron microscopy of PV_{dis} tissues (Figure 8B and 8C). Furthermore, SHR PV myocytes also exhibited changes in the lateral sarcolemma ultrastructure. Whereas Wistar myocytes had a relatively convoluted surface, with caveolae clustering within outcroppings of membrane (see electron micrographs in Figure 8B, solid red line), SHR myocytes displayed straighter sarcolemma characterized by a smaller "convolution index" (L/L_o-1, where L is the length of membrane contour, and L_o is the shortest length connecting end points of membrane segment; Figure 8D),[33] which indicates caveolae flattening in response to elevated stretch in SHRs.

Discussion

Cardiac stretch has previously been shown to modulate several vulnerable electrophysiological parameters in PV myocytes, potentially contributing to the development of AF.[6,7] However, the molecular mechanisms of cardiac mechanoelectrical transduction remain poorly understood. In this study, we provided conceptual innovation of mechanosensing in the heart, linking specialized cell structures, caveolae, and their response to stretch to the activation of mechanosensitive $I_{Cl,swell}$. We showed that pathological activation of $I_{Cl,swell}$ modulates electrical activity in the PVs, promoting the development of ectopic foci and triggering AF.

The role of caveolae in mechanosensing has been demonstrated in various cell types, including cardiomyocytes. Caveolae flattening and the incorporation of caveolar membrane into the plasma membrane in response to stretch plays a crucial role in cell volume regulation. Our results showing decreased mechanoprotection of SHR PV myocytes agrees with findings that caveolae act as membrane convolutions that can flatten in response to increased membrane tension, thereby serving as a buffer to prevent membrane rupture.[33,34] In addition, evidence has accumulated for the existence of active signaling from caveolae in response to changes in mechanical forces; for example, stretch activation of caveolae-associated $I_{Cl,swell}$ was linked to the regulation of cellular contractility, thus adjusting cardiac performance on changes in blood volume of the heart.[10,15] In addition, caveolae are essential for angiotensin II type 1 receptor–mediated atrial natriuretic peptide secretion[35] and have been shown to be involved in the production of reactive oxygen species and nitric oxide via activation of NADPH oxidase subunits and eNOS.[36] In the healthy heart, these signaling pathways provide balancing feedback to regulate cardiac performance on increased BP. However, under disease conditions associated with pathological stretch, disruption of caveolae and activation of caveolar signaling pathways might be proarrhythmic, as demonstrated in the present study.

Pathological stretch-induced activation of $I_{Cl,swell}$ depolarized RP toward the equilibrium potential for Cl^- (between −65 and −40 mV[37]; Figure 2). Such depolarization was most prominent in PV_{dis} due to ≈40% decreased density of I_{K1} compared with the LA myocardium.[30] $I_{Cl,swell}$-induced RP depolarization up to −60 mV shifts a significant proportion of fast sodium channels into an inactivated state, which in turn suppresses conduction velocity and leads to the development of conduction block proximally in the PV. Therefore, conduction block is induced by stretch more proximally in the PV, where Cl^- currents cannot be compensated by the I_{K1}. Acute (7.2±1.6 mm Hg) atrial stretch–induced conduction slowing across the PV-LA junction and enhanced electrogram signal complexity, which likely suggests the presence of intra-PV conduction blocks, were observed in humans who underwent evaluation of the right superior PV–LA junction using an epicardial mapping plaque.[7] Similarly, pronounced repolarization heterogeneity as well as nonsustained reentrant activity was observed by Arora et al in coronary-perfused, isolated,

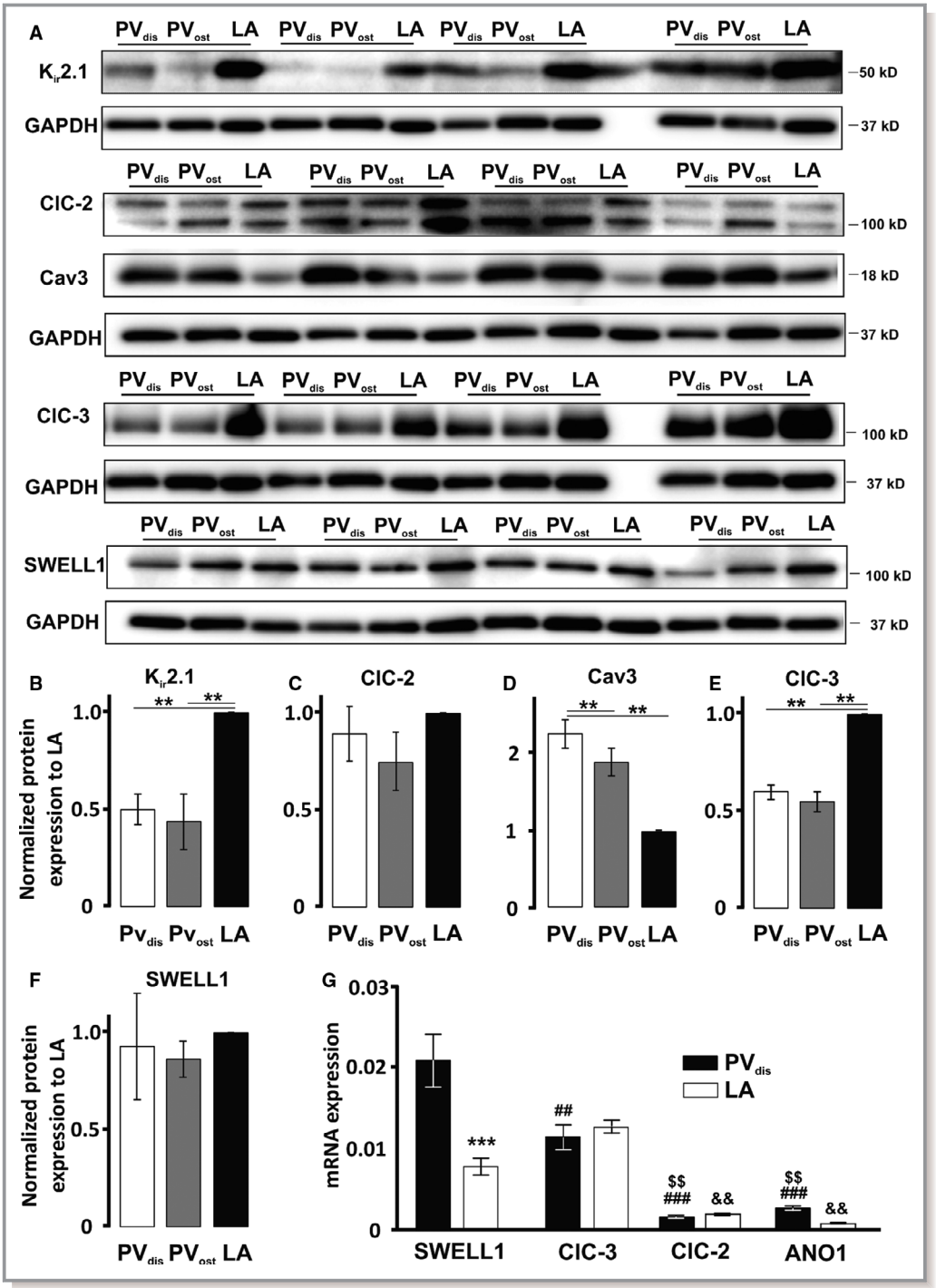

Figure 6. Expression of chloride channels CIC-2, CIC-3, and SWELL1, caveolar scaffolding protein caveolin 3 (Cav3), and potassium channel $K_{ir}2.1$ along the pulmonary vein (PV) vs left atrium (LA). **A**, Protein expression levels of $K_{ir}2.1$, CIC-2, Cav3, CIC-3, and SWELL1 measured in PV distal (PV_{dis}), PV ostium (PV_{ost}), and LA from the same rat (n=4). **B** through **F**, Corresponding protein expression levels normalized to GAPDH (n=4 per group). $^{**}P<0.01$ by 1-way ANOVA with Bonferroni correction. **G**, Comparative analysis of mRNA expression levels for sarcolemmal chloride ion channel isoforms normalized to GAPDH. n=6 per region for SWELL1 and n=5 per region for CIC-2, CIC-3, and ANO1. $^{***}P<0.01$ vs PV_{dis} for SWELL1; $^{\#\#}P<0.01$, $^{\#\#\#}P<0.001$ vs SWELL1 for PV_{dis}; $^{\$\$}P<0.01$ vs CIC-3 for PV_{dis}; and $^{\&\&}P<0.01$ vs CIC-3 for LA by 2-way ANOVA with Bonferroni correction. ANO1 indicates anoctamin 1; Cav3, caveolin 3; CIC, chloride channel; SWELL1, also known as LRRC8A (leucine rich repeat containing protein 8A).

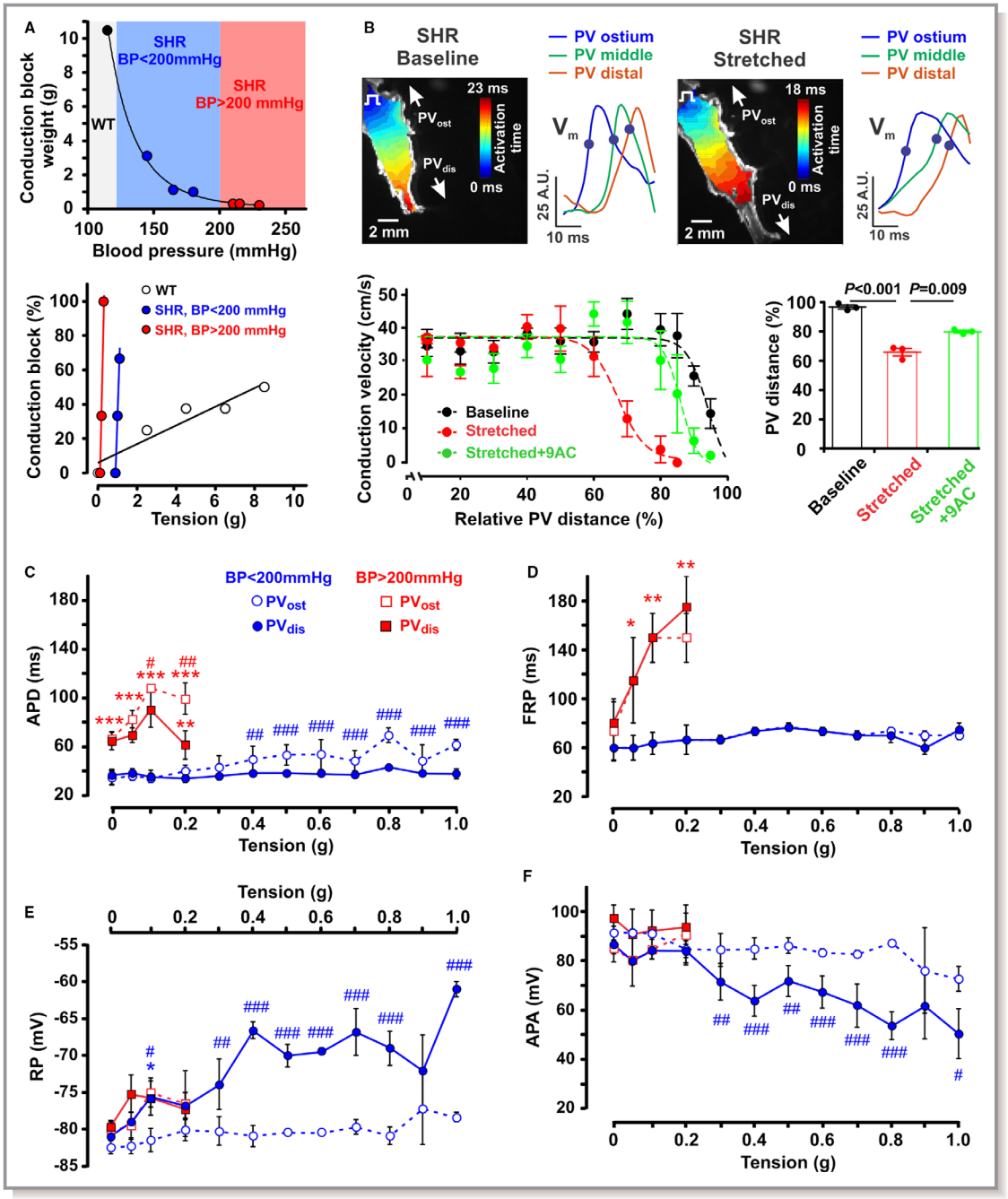

Figure 7. Effect of stretch on electrical activity of the pulmonary vein (PV) in spontaneously hypertensive rats (SHRs). **A**, Development of intra-PV conduction block in SHRs. (Top) Negative exponential dependence between the aortic blood pressure (BP) and the maximal tension required to induce intra-PV conduction block in normotensive rats (Wistar [WT]; black dots) and SHRs with BP <200 mm Hg (blue dots) and BP >200 mm Hg (red dots). (Bottom) Probability of intra-PV conduction block estimated at different tensions applied to WT (n=8) and SHRs with BP <200 mm Hg and BP >200 mm Hg. **B**, (Top) PV activation maps and superimposed upstrokes of optical action potentials (V_m) recorded along the PV are shown for baseline (left) and pathological stretch (right) conditions in SHRs. (Bottom) Distribution of conduction velocity along the PV (left) and relative PV distance (in percentage from the PV length; right) activated at baseline, during stretch, and after application of swelling-activated chloride ion channel ($I_{Cl,swell}$) blocker 9AC (9-anthracenecarboxylic acid) are shown (n=4 per group). *P values were determined by 2-way ANOVA with Bonferroni correction. **C** through **F**, Stretch-induced changes in active potential (AP) parameters are shown for 2 groups of SHRs based on their BP. *P<0.05, **P<0.01, **P<0.01 vs SHR with BP <200 mm Hg, and $^{\#}P$<0.05, $^{\#\#}P$<0.01, $^{\#\#\#}P$<0.001 for PV distal (PV_{dis}) vs PV ostium (PV_{ost}) by repeated measurements 2-way ANOVA with Bonferroni correction. APA indicates action potential amplitude; APD, action potential duration; FRP, functional refractory period.

whole-atrial canine preparations using optical mapping.[22] The authors highlighted that reentry occurred more distally in the PV, whereas focal activity seemed to occur more proximally, with which the results observed in our study agree. A recent case report on a patient who underwent a radiofrequency ablation of drug-refractory paroxysmal AF described intra-PV echo beats characterized by PV automaticity with a delayed, stably coupled second component suggesting a small reentry within the vein.[38]

The molecular composition responsible for cardiac $I_{Cl,swell}$ remains questionable and highly controversial. This also seems to depend on the type of cardiac tissues studied. Xiong et al used cardiac-specific, inducible ClC-3 gene deletion, which eliminated a native volume-sensitive chloride current in both atrial and ventricular mouse myocytes.[26] Meanwhile, the same group demonstrated a functional presence of ClC-2 chloride inward rectifier channels in cardiac sinoatrial nodal guinea pig pacemaker cells.[25] Although no experimental data are available to date on a functional presence of ClC-2 or ClC-3 channels in PV myocytes, one could suggest that, considering that PV myocytes represent electrophysiological properties of both atrial and pacemaker cells (the presence of spontaneous electrical activity[19,39,40] and a low membrane RP stabilizing K^+ current I_{K1}[24,40] associated with a decreased expression of $K_{ir}2.x$ channels[30]), both ClC-2 and ClC-3 channels may contribute, at different proportions, to PV $I_{Cl,swell}$.

We also detected, for the first time, the presence of SWELL1 channels in the rat and human myocardium, at both mRNA and protein levels (Figures 4, 5, 6A, and 6G). SWELL1 is a recently characterized chloride channel and may represent an essential component of volume-regulated anion current in noncardiac cells.[27] SWELL1 mRNA was detected broadly in mouse tissues.[27] Although SWELL1 mRNA expression has been detected in the heart, neither protein expression or localization nor functional contribution of these channels into cardiac $I_{Cl,swell}$ were reported. Our comparative reverse transcription quantitative polymerase chain reaction analysis showed that that SWELL1 and ClC-3 channels demonstrate an equal abundance in both PV and LA myocardium (Figure 6G). Therefore, it is possible that SWELL1 channels could also functionally contribute to PV $I_{Cl,swell}$. Based on our coimmunoprecipitation (Figure 5) and coimmunofluorescence (Figure 4) analysis, SWELL1 channels might be involved in caveolar mechanosensitive complex and thus participate in stretch-induced PV arrhythmogenesis and hypertensive-associated remodeling.

Compared with biophysical properties of ClC-2, ClC-3 and SWELL1 channels, cardiac $I_{Cl,swell}$ recorded in native PV myocytes and hiPS-CMs (Figure 3) demonstrate outward rectification similar to both ClC-3[26] and SWELL1[27] channels. In contrast, ClC-2 channels show a prominent inward rectification which was not seen in the $I_{Cl,swell}$ recorded in the present study. Assuming a 10-fold smaller ClC-2 mRNA expression level compared with that for ClC-3 and SWELL1 (Figure 6G), it is unlikely that ClC-2 current, if functionally present, plays an important role in the PV $I_{Cl,swell}$.

In the present study, higher sensitivity of SHR PV to stretch-induced RP depolarization and intra-PV conduction dissociation was associated with decreased Cav3 protein expression level and downregulation of caveolae structures (Figure 8). Although the exact mechanisms of activation of $I_{Cl,swell}$ in response to stretch remain unknown, their interaction with caveolae appears to be critical for channel activation.[10] It has been previously shown that ClC-2 channels are concentrated in lipid rafts in basal condition and relocalize to the cell surface membrane on caveolae disruption via cholesterol depletion, with a subsequent increase in their activity.[28] The same might be true for ClC-3 and SWELL1 channels. This is supported by our data on basal changes in AP morphology in SHR PVs (Figure S10) and their higher sensitivity to stretch which could indicate constitutively active $I_{Cl,swell}$ and/or greater $I_{Cl,swell}$ activated by a lower level of stretch in SHRs versus Wistar rats.

We found that SHR sensitivity to stretch depended on the rat's BP. Although all SHRs had a significantly higher sensitivity to stretch than the Wistar group, rats with BP >200 mm Hg showed RP depolarization and intra-PV conduction block at much smaller weights compared with SHRs with BP <200 mm Hg (Figure 7). It has been shown that SHRs develop hypertension at 2 to 3 months of age and that it peaks from 6 months of age onward with increasing compensatory concentric cardiac hypertrophy (12–15 months) before the onset of heart failure at the age older than 18 months.[41] Significant atrial remodeling, including biatrial hypertrophy, elevated atrial fibrosis, and increased atrial arrhythmogenesis, has been observed in SHRs.[42] Importantly, as it was described in a study by Bing et al, ≈60% of SHRs developed evidence of cardiac decompensation, another 13% survived to 24 months and did not have evidence of heart failure, and the rest died for noncardiac reasons (eg, stroke, debilitation, tumor).[41] Because the magnitude and duration of hypertension are important determinants of the degree of hypertrophy and the functional status of ventricles, it may result in the different degrees of atrial remodeling and explain the observed sensitivity in 2 groups of SHRs. Therefore, it may result in the different degree of atrial and PVs remodeling and explain the observed distinct sensitivity in 2 groups of SHRs. Further studies are required to explore the cellular and molecular mechanisms behind the observed phenotypes, which might be related to the differences in ion channel expression repertoire and/or calcium handling.

Clinical Perspectives

Although some forms of AF can be successfully treated via PV isolation, the success rate of such procedures for individuals

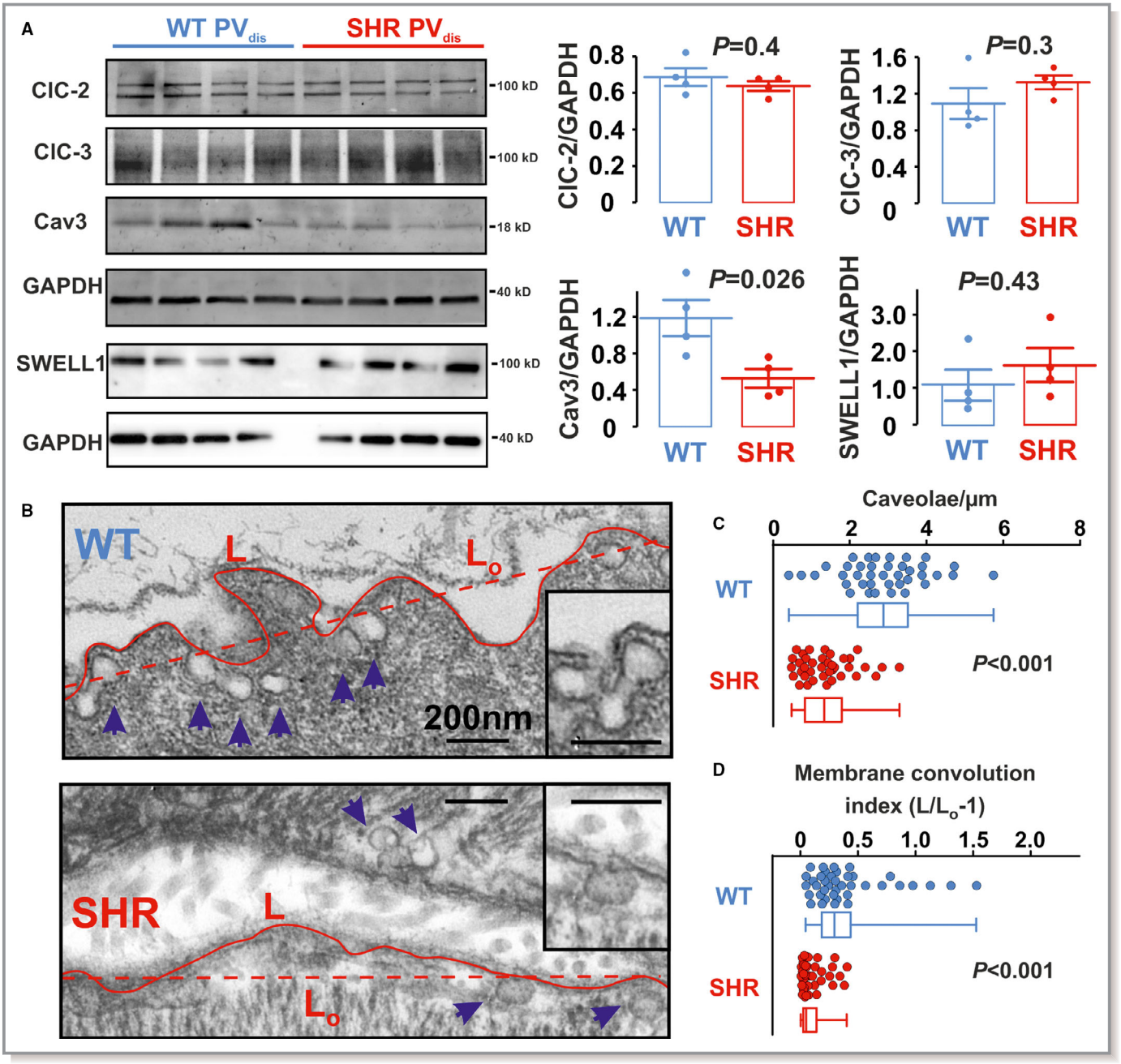

Figure 8. Molecular and structural remodeling of caveolar mechanosensitive complex. **A**, Immunoblots for CIC-2, CIC-3, SWELL1, and Cav3 from Wistar (WT; n=4) and spontaneously hypertensive rat (SHR; n=4) pulmonary vein distal (PV_{dis}) tissues. Expression levels were normalized to GAPDH. *P* values were determined by unpaired Student *t* test. **B**, Downregulation of Cav3 correlates with elevated membrane tension and disruption of caveolae structures during hypertension. Representative composite electron micrographs showing the lateral sarcolemmal membranes of cardiomyocytes from nonstretched WT and SHR PV_{dis} tissues. Blue arrowheads denote caveolae connected to plasma membrane (scale bars=200 nm). **C** and **D**, Quantification of caveolae density, normalized to membrane length (**C**), and membrane convolution index (L/L_o-1) (**D**), n=40 cells per group. Box plots show medians with interquartile range; whiskers represent fifth and 95th percentile; each point represents 1 micrograph. *P* values were determined by unpaired Student *t* test. Cav3 indicates caveolin 3; CIC, chloride channel; L, length of membrane contour; L_o, shortest length connecting end points of membrane segment; SWELL1, also known as LRRC8A (leucine rich repeat containing protein 8A).

with persistent AF is poor (≈50%).[43] The relatively poor response to conventional treatment is attributed to the extensive remodeling of the atrial myocardium, which creates multiple ectopic foci and confounds strategies for identifying ablation targets.[44] Furthermore, catheter ablation empirically destroys viable atrial tissue rather than directly addressing

the underlying triggering mechanisms of AF. To improve outcomes, both pharmacological and gene therapy should be considered as alternative approaches for AF treatment and prevention. Our study introduces a novel paradigm by which electrophysiological changes occur secondary to cellular structural remodeling. This extends beyond the classical concept of electrical remodeling and adds a new dimension to cardiovascular disease, providing a basis from which to develop novel and effective therapeutic approaches targeted to treat stretch-induced arrhythmogenesis and AF by preventing the degradation or promoting the restoration of cardiac cytoarchitecture.

Study Limitations

Our study demonstrates that $I_{Cl,swell}$ likely consists of at least 2 currents produced by mechanosensitive ClC-3 and SWELL1 channels, and ClC-2 current, if functionally present, plays an important role in the PV $I_{Cl,swell}$. Unfortunately, isoform-selective pharmacological inhibitors of mechanosensitive chloride channels are not currently available, and cardiac-specific and isoform-selective knockout animals are required to dissect the exact molecular composition of $I_{Cl,swell}$ current measured in PVs. These experiments are outside of the scope of the present study, which reports, for the first time, important findings on the role of caveolae-associated stretch-activated $I_{Cl,swell}$ in PV arrhythmogenesis, and will be reported in our follow-up studies.

Mechanosensitivity has been reported for multiple ion channels, including specific K^+-selective stretch-activated channels such as TREK and TREK-like channels, BK channels, cation nonselective stretch-activated channels (Piezo and transient receptor potential channels), and Cl^- channels.[9,45–47] In addition, stretch can directly modulate biophysical properties and functioning of multiple voltage- and ligand-gated ion channels including K_v and K_{ir} potassium channels, $Na_v1.5$ sodium channels, and $Ca_v1.2$ calcium channels, thus modulating AP morphology.[45] Therefore, it is possible that other ion channels may contribute to stretch-induced AP changes in the PV myocardium. However, as demonstrated in our study, $I_{Cl,swell}$ has a key role in RP depolarization and conduction dissociation in PV, which could be abolished via selective pharmacological inhibition of $I_{Cl,swell}$ by DCPIB, DIDS, and 9AC. It is unlikely that all of these agents could augment outward potassium current to counteract $I_{Cl,swell}$ and hyperpolarize RP.

Acknowledgments

We are grateful for technical assistance with electron microscopy studies from Benjamin August (University of Wisconsin School of Medicine Electron Microscope Facility) and for functional animal assessment performed by Dr Timothy Hacker (University of Wisconsin–Madison Animal Physiology Core Facility).

Sources of Funding

This work was supported by the Russian Foundation for Basic Research Grants 14-04-01781 and 17-04-01634 (to Rosenshtraukh), National Institutes of Health (NIH) 1RO1HL141214-01, American Heart Association (AHA) 16SDG29120011, and the Wisconsin Partnership Program 4140 (to Glukhov), and AHA Fellowship 17POST33370089 (to Lang). Turner would like to acknowledge NIH predoctoral training grant T32GM008688.

Disclosures

Schmuck and Raval have ownership and financial interest in Cellular Logistics Inc. The remaining authors have no disclosures to report.

References

1. Schotten U, Verheule S, Kirchhof P, Goette A. Pathophysiological mechanisms of atrial fibrillation: a translational appraisal. *Physiol Rev*. 2011;91:265–325.
2. Benjamin EJ, Levy D, Vaziri SM, D'Agostino RB, Belanger AJ, Wolf PA. Independent risk factors for atrial fibrillation in a population-based cohort. The Framingham Heart Study. *JAMA*. 1994;271:840–844.
3. Haissaguerre M, Jais P, Shah DC, Takahashi A, Hocini M, Quiniou G, Garrigue S, Le Mouroux A, Le Metayer P, Clementy J. Spontaneous initiation of atrial fibrillation by ectopic beats originating in the pulmonary veins. *N Engl J Med*. 1998;339:659–666.
4. Tabatabaei N, Asirvatham SJ. Supravalvular arrhythmia: identifying and ablating the substrate. *Circ Arrhythm Electrophysiol*. 2009;2:316–326.
5. Sadek MM, Maeda S, Chik W, Santangeli P, Zado ES, Schaller RD, Supple GE, Frankel DS, Hutchinson MD, Garcia FC, Riley MP, Lin D, Dixit S, Callans DJ, Marchlinski FE. Recurrent atrial arrhythmias in the setting of chronic pulmonary vein isolation. *Heart Rhythm*. 2016;13:2174–2180.
6. Ravelli F. Mechano-electric feedback and atrial fibrillation. *Prog Biophys Mol Biol*. 2003;82:137–149.
7. Walters TE, Lee G, Spence S, Larobina M, Atkinson V, Antippa P, Goldblatt J, O'Keefe M, Sanders P, Kistler PM, Kalman JM. Acute atrial stretch results in conduction slowing and complex signals at the pulmonary vein to left atrial junction: insights into the mechanism of pulmonary vein arrhythmogenesis. *Circ Arrhythm Electrophysiol*. 2014;7:1189–1197.
8. Chang SL, Chen YC, Chen YJ, Wangcharoen W, Lee SH, Lin CI, Chen SA. Mechanoelectrical feedback regulates the arrhythmogenic activity of pulmonary veins. *Heart*. 2007;93:82–88.
9. Seol CA, Kim WT, Ha JM, Choe H, Jang YJ, Youm JB, Earm YE, Leem CH. Stretch-activated currents in cardiomyocytes isolated from rabbit pulmonary veins. *Prog Biophys Mol Biol*. 2008;97:217–231.
10. Kozera L, White E, Calaghan S. Caveolae act as membrane reserves which limit mechanosensitive I(Cl, swell) channel activation during swelling in the rat ventricular myocyte. *PLoS One*. 2009;4:e8312.
11. Pfeiffer ER, Wright AT, Edwards AG, Stowe JC, McNall K, Tan J, Niesman I, Patel HH, Roth DM, Omens JH, McCulloch AD. Caveolae in ventricular myocytes are required for stretch-dependent conduction slowing. *J Mol Cell Cardiol*. 2014;76:265–274.
12. Gabella G. Inpocketings of the cell membrane (caveolae) in the rat myocardium. *J Ultrastruct Res*. 1978;65:135–147.
13. Gilbert G, Ducret T, Savineau JP, Marthan R, Quignard JF. Caveolae are involved in mechanotransduction during pulmonary hypertension. *Am J Physiol Lung Cel Mol Physiol*. 2016;310:L1078–L1087.
14. Parton RG, Simons K. The multiple faces of caveolae. *Nat Rev Mol Cell Biol*. 2007;8:185–194.
15. Vandenberg JI, Bett GC, Powell T. Contribution of a swelling-activated chloride current to changes in the cardiac action potential. *Am J Physiol*. 1997;273:C541–C547.
16. Markandeya YS, Phelan LJ, Woon MT, Keefe AM, Reynolds CR, August BK, Hacker TA, Roth DM, Patel HH, Balijepalli RC. Caveolin-3 overexpression attenuates cardiac hypertrophy via inhibition of T-type Ca^{2+} current modulated

by protein kinase Cα in cardiomyocytes. *J Biol Chem*. 2015;290:22085–22100.

17. Piech A, Dessy C, Havaux X, Feron O, Balligand JL. Differential regulation of nitric oxide synthases and their allosteric regulators in heart and vessels of hypertensive rats. *Cardiovasc Res*. 2003;57:456–467.
18. Reilly SN, Liu X, Carnicer R, Recalde A, Muszkiewicz A, Jayaram R, Carena MC, Wijesurendra R, Stefanini M, Surdo NC, Lomas O, Ratnatunga C, Sayeed R, Krasopoulos G, Rajakumar T, Bueno-Orovio A, Verheule S, Fulga TA, Rodriguez B, Schotten U, Casadei B. Up-regulation of miR-31 in human atrial fibrillation begets the arrhythmia by depleting dystrophin and neuronal nitric oxide synthase. *Sci Transl Med*. 2016;8:340ra74.
19. Egorov YV, Kuz'min VS, Glukhov AV, Rosenshtraukh LV. Electrophysiological characteristics, rhythm, disturbances and conduction discontinuities under autonomic stimulation in the rat pulmonary vein myocardium. *J Cardiovasc Electrophysiol*. 2015;26:1130–1139.
20. Lang D, Glukhov AV. High-resolution optical mapping of the mouse sino-atrial node. *J Vis Exp*. 2016;118:e54773.
21. Zhang J, Wilson GF, Soerens AG, Koonce CH, Yu J, Palecek SP, Thomson JA, Kamp TJ. Functional cardiomyocytes derived from human induced pluripotent stem cells. *Circ Res*. 2009;104:e30–e41.
22. Arora R, Verheule S, Scott L, Navarrete A, Katari V, Wilson E, Vaz D, Olgin JE. Arrhythmogenic substrate of the pulmonary veins assessed by high-resolution optical mapping. *Circulation*. 2003;107:1816–1821.
23. Clemo HF, Stambler BS, Baumgarten CM. Swelling-activated chloride current is persistently activated in ventricular myocytes from dogs with tachycardia-induced congestive heart failure. *Circ Res*. 1999;84:157–165.
24. Ehrlich JR, Cha TJ, Zhang L, Chartier D, Melnyk P, Hohnloser SH, Nattel S. Cellular electrophysiology of canine pulmonary vein cardiomyocytes: action potential and ionic current properties. *J Physiol*. 2003;551:801–813.
25. Huang ZM, Prasad C, Britton FC, Ye LL, Hatton WJ, Duan D. Functional role of CLC-2 chloride inward rectifier channels in cardiac sinoatrial nodal pacemaker cells. *J Mol Cell Cardiol*. 2009;47:121–132.
26. Xiong D, Heyman NS, Airey J, Zhang M, Singer CA, Rawat S, Ye L, Evans R, Burkin DJ, Tian H, McCloskey DT, Valencik M, Britton FC, Duan D, Hume JR. Cardiac-specific, inducible ClC-3 gene deletion eliminates native volume-sensitive chloride channels and produces myocardial hypertrophy in adult mice. *J Mol Cell Cardiol*. 2010;48:211–219.
27. Qiu Z, Dubin AE, Mathur J, Tu B, Reddy K, Miraglia LJ, Reinhardt J, Orth AP, Patapoutian A. SWELL1, a plasma membrane protein, is an essential component of volume-regulated anion channel. *Cell*. 2014;157:447–458.
28. Hinzpeter A, Fritsch J, Borot F, Trudel S, Vieu DL, Brouillard F, Baudouin-Legros M, Clain J, Edelman A, Ollero M. Membrane cholesterol content modulates ClC-2 gating and sensitivity to oxidative stress. *J Biol Chem*. 2007;282:2423–2432.
29. Trouet D, Hermans D, Droogmans G, Nilius B, Eggermont J. Inhibition of volume-regulated anion channels by dominant-negative caveolin-1. *Biochem Biophys Res Commun*. 2001;284:461–465.
30. Melnyk P, Ehrlich JR, Pourrier M, Villeneuve L, Cha TJ, Nattel S. Comparison of ion channel distribution and expression in cardiomyocytes of canine pulmonary veins versus left atrium. *Cardiovasc Res*. 2005;65:104–116.
31. Choisy SC, Arberry LA, Hancox JC, James AF. Increased susceptibility to atrial tachyarrhythmia in spontaneously hypertensive rat hearts. *Hypertension*. 2007;49:498–505.
32. Patel DG, Higgins RS, Baumgarten CM. Swelling-activated cl current, ICl, swell, is chronically activated in diseased human atrial myocytes. *Biophys J*. 2003;84:233a.
33. Wei EQ, Sinden DS, Mao L, Zhang H, Wang C, Pitt GS. Inducible Fgf13 ablation enhances caveolae-mediated cardioprotection during cardiac pressure overload. *Proc Natl Acad Sci USA*. 2017;114:E4010–E4019.
34. Sinha B, Koster D, Ruez R, Gonnord P, Bastiani M, Abankwa D, Stan RV, Butler-Browne G, Vedie B, Johannes L, Morone N, Parton RG, Raposo G, Sens P, Lamaze C, Nassoy P. Cells respond to mechanical stress by rapid disassembly of caveolae. *Cell*. 2011;144:402–413.
35. Oh YB, Gao S, Lim JM, Kim HT, Park BH, Kim SH. Caveolae are essential for angiotensin II type 1 receptor-mediated ANP secretion. *Peptides*. 2011;32:1422–1430.
36. Yang B, Rizzo V. TNF-α potentiates protein-tyrosine nitration through activation of NADPH oxidase and eNOS localized in membrane rafts and caveolae of bovine aortic endothelial cells. *Am J Physiol Heart Circ Physiol*. 2007;292:H954–H962.
37. Baumgarten CM, Fozzard HA. Intracellular chloride activity in mammalian ventricular muscle. *Am J Physiol*. 1981;241:C121–C129.
38. Bun SS, Latcu DG, Wedn AM, Saoudi N. Intrapulmonary vein "echo" beats. *HeartRhythm Case Rep*. 2018;4:464–465.
39. Tsuneoka Y, Kobayashi Y, Honda Y, Namekata I, Tanaka H. Electrical activity of the mouse pulmonary vein myocardium. *J Pharmacol Sci*. 2012;119:287–292.
40. Tsuneoka Y, Irie M, Tanaka Y, Sugimoto T, Kobayashi Y, Kusakabe T, Kato K, Hamaguchi S, Namekata I, Tanaka H. Permissive role of reduced inwardly-rectifying potassium current density in the automaticity of the guinea pig pulmonary vein myocardium. *J Pharmacol Sci*. 2017;133:195–202.
41. Bing OH, Brooks WW, Robinson KG, Slawsky MT, Hayes JA, Litwin SE, Sen S, Conrad CH. The spontaneously hypertensive rat as a model of the transition from compensated left ventricular hypertrophy to failure. *J Mol Cell Cardiol*. 1995;27:383–396.
42. Lau DH, Shipp NJ, Kelly DJ, Thanigaimani S, Neo M, Kuklik P, Lim HS, Zhang Y, Drury K, Wong CX, Chia NH, Brooks AG, Dimitri H, Saint DA, Brown L, Sanders P. Atrial arrhythmia in ageing spontaneously hypertensive rats: unraveling the substrate in hypertension and ageing. *PLoS One*. 2013;8:e72416.
43. Verma A, Jiang CY, Betts TR, Chen J, Deisenhofer I, Mantovan R, Macle L, Morillo CA, Haverkamp W, Weerasooriya R, Albenque JP, Nardi S, Menardi E, Novak P, Sanders P. Approaches to catheter ablation for persistent atrial fibrillation. *N Engl J Med*. 2015;372:1812–1822.
44. Oakes RS, Badger TJ, Kholmovski EG, Akoum N, Burgon NS, Fish EN, Blauer JJ, Rao SN, DiBella EV, Segerson NM, Daccarett M, Windfelder J, McGann CJ, Parker D, MacLeod RS, Marrouche NF. Detection and quantification of left atrial structural remodeling with delayed-enhancement magnetic resonance imaging in patients with atrial fibrillation. *Circulation*. 2009;119:1758–1767.
45. Peyronnet R, Nerbonne JM, Kohl P. Cardiac mechano-gated ion channels and arrhythmias. *Circ Res*. 2016;118:311–329.
46. Okamoto Y, Kawamura K, Nakamura Y, Ono K. Pathological impact of hyperpolarization-activated chloride current peculiar to rat pulmonary vein cardiomyocytes. *J Mol Cell Cardiol*. 2014;66:53–62.
47. Kamkin A, Kiseleva I, Wagner KD, Bohm J, Theres H, Gunther J, Scholz H. Characterization of stretch-activated ion currents in isolated atrial myocytes from human hearts. *Pflugers Arch*. 2003;446:339–346.

SUPPLEMENTAL MATERIAL

Data S1.

Supplemental Methods

Ethical approval

All experiments were conducted in accordance with the National Institutes of Health Guide for the Care and Use of Laboratory Animals (NIH Pub. No. 80-23). All methods and protocols used in these studies have been approved by the Animal Care and Use Committee of the Cardiology Research Center (Moscow, Russia) and University of Wisconsin-Madison (U.S.A.) following the Guidelines for Care and Use of Laboratory Animals published by NIH (publication No. 85-23, revised 1996). All animals used in this study received humane care in compliance with the Guide for the Care and Use of Laboratory Animals.

Human heart collection protocols were approved by the University of Wisconsin Institutional Review Board. Non-failing human hearts that went unused for organ transplant were obtained from the University of Wisconsin Organ Procurement Organization, Madison, WI. At the time of harvest, hearts were aseptically excised, perfused and stored in cold cardioplegia solution, and transported on ice as described previously in details.[1-3] Human left atrial tissue was used for co-immunoprecipitation (**Figure S8**) and co-immunohistochemical experiments (**Figure 4**).

Echocardiography

Systolic and diastolic function was assessed by echocardiographic examination in lightly anesthetized (1.5% isoflurane) rats using the a 17.5-MHz transducer (RMV 707B; Visual Sonics, Toronto, ON, Canada), as previously described.[4] Two-dimensional M-Mode images were recorded both in the short and long axes. Average values were obtained from the measurement of 3-5 consecutive cardiac cycles. Blood pressure was measured using tail cuff plethysmography (Harvard Apparatus Ltd) from lightly anesthetized rats.

Animals

Adult (8-12 month old) Wistar rats (n=62) and spontaneously hypertensive rats (n=17) were anesthetized with isoflurane (induced at 3-5% and maintained at 1-3%) to assure the appropriate

level of anesthesia by checking the loss of pain reflex. The isolated pulmonary veins (PV) preparation was performed as described previously.[5] Briefly, after mid-sternal incision, the heart with lungs was removed and placed in oxygenated (95% O_2, 5% CO_2) room-temperature Tyrode solution of the following composition (in mmol/L): 118 NaCl, 1.8 $CaCl_2$, 1.2 $MgCl_2.6H_2O$, 4.7 KCl, 1.2 NaH_2PO_4, 25 $NaHCO_3$, and 11 glucose (pH=7.35±0.05). While bathed in the same solution, lung, thymus, and fat tissue were dissected and removed. The left atrium together with the left atrial appendage and PV region was dissected from the ventricles, right atrium, and inter-atrial septum. The preparation then was placed in a tissue bath (2.5 mL) and continuously superfused with oxygenated Tyrode's solution (18 ml/min). The temperature was gradually increased with a rate of 1°C per min to 37 ± 0.5°C. Central PV was cleaned from fat and lung tissues, adjacent to the left atrium, lanced and then positioned on a thin coat of silicon on the bottom of a tissue bath with the endocardial side facing upward. The pacing electrode was placed on the edge of the left atrial appendage.

Microelectrode recordings

Measurements were performed after 40-60 minutes from the isolation procedure. Transmembrane potentials were simultaneously recorded from the endocardial surface of the distal (PV_{dis}) and the ostium (PV_{ost}) part of the PV by using two glass microelectrodes filled with 3.0 mmol/L KCl (tip resistance ~10-40 MΩ), and connected to high-input impedance amplifiers (WPI model KS-701, World Precision Instruments, New Haven, CT, U.S.A.). Transmembrane potential signals were recorded, digitalized (sampling rate of 5 kHz) by using analog-digital converter (E-154, L-Card, Moscow, Russia) and then saved on a computer for offline analysis as described previously [5]. To characterize electrophysiological properties of the vein myocardium, resting potential (RP), action potential (AP) amplitude (APA) and action potential duration at 90% repolarization (APD) were measured during baseline pacing. Stimulation electrodes were positioned on the left atrial appendage. Baseline pacing cycle length (S1S1) was 300 ms. The pacing current was at least 2× the pacing threshold.

To explore the dynamic changes in AP characteristics, APD restitution curves (the dependency of APD on the preceding diastolic interval, DI) were measured using an S1S1 stimulation protocol [6]. Briefly, basic S1S1 stimulation was delivered for at least 1 min. APD of the last paced AP was

measured. Pacing was then reinitiated at a shorter S1S1 cycle length, and APD was determined after at least 1 min stimulation at new S1S1. The S1S1 was shortened from 300 ms to 200 ms, and then to 150 ms, 120 ms, and 100 ms and then further in steps of 10 ms until 1:1 capture failed. The shortest pacing S1 interval to capture without Wenckebach periodicity was deemed the functional refractory period (FRP). After termination of pacing protocol, the preparation recovered during 15 min and constant pacing of S1S1=300 ms. DI was calculated as a difference between the S1S1 period (a time interval between the AP_N and AP_{N+1}) and APD measured for AP_N. The maximal slope of the APD restitution curve was calculated as a first derivative of the fitted curve for each DI.

Experimental protocols

The following experimental series were performed on WT rats:

1. **Physiological stretch (n=8)**: 0 – 1.5 g of applied weight corresponding to a physiological pulmonary venous pressure range from 0 to ~4 mmHg (calculated as applied weight x gravity constant/cross section area of the PV preparation). First, baseline recordings were performed and dynamic restitution protocol was applied without stretch. The preparation then recovered for 15 min with constant pacing S1S1=300 ms. After that in PV preparations, electrical stimulation was stopped and spontaneous activity was measured, if present. Then a progressively increased stretch was applied by using weight blocks connected to the distal part of the vein. The applied weight was progressively increased from 0.1 g to 0.2 g, 0.3 g and then to 1.5 g. For each weight, dynamic restitution protocol was applied as described above. For adaptation, each weight was applied for at least 60 min prior the measurements.
2. **Pathological stretch (n=8)**: 2.5 – 10.5 g of weight corresponding to a pathological pressure range from ~6 to 26 mmHg. Similar to physiological stretch protocol, baseline recordings were performed and dynamic restitution protocol was applied without stretch. The preparation then recovered for 15 min with constant pacing S1S1=300 ms. After that in PV preparations, electrical stimulation was stopped and spontaneous activity was measured, if present. Then a progressively increased stretch was applied by using weight blocks connected to the distal part of the vein. The applied weight was progressively increased to

2.5 g, 4.5 g, 6.5 g, 8.5 g and 1.5 g. For each weight, dynamic restitution protocol was applied as described above. For adaptation, each weight was applied for at least 60 min prior the measurements.

3. **Pathological stretch + DIDS (n=7)**. In a separate series of experiments, a role of $I_{Cl,swell}$ in stretch-induced RP depolarization and intra-PV conduction dissociation was estimated. After 30-40 min adaptation period, preparations were exposed to 10.5 g weight for at least 60 min. After that, a presence of intra-PV conduction block was determined (i.e. RP above -60 mV and APA less than 20 mV). If no block occurred, the weight was increased by 1 g and then it was applied for 30-60 min, based on AP changed during the continuous microelectrode recording. The procedure was repeated until conduction block occurred. The maximal applied weight was 13.5 g. When conduction block occurred, a non-selective inhibitor of $I_{Cl,swell}$ DIDS (100 μM) was applied.
4. **Pathological stretch + DCPIB (n=9)**. Similar to previous protocol #3, applied weight was adjusted to induce intra-PV conduction dissociation, and then selective $I_{Cl,swell}$ inhibitor DCPIB (100 μM) was applied.
5. **Optical mapping of intra-PV conduction dissociation (n=4)**. Similar to protocols #3 and #4, applied weight was adjusted to induce intra-PV conduction dissociation, and then non-selective $I_{Cl,swell}$ inhibitor 9AC (100 μM) was applied.

Optical mapping

To analyze spatial changes in AP morphology along the PV and study dynamics of intra-PV conduction dissociation, the entire cental rat PV was stained by immersing the tissue in Tyrode's solution containing the voltage-sensitive indicator RH237 (10 μM; ThermoFisher Scientific) for at least 15 min at room temperature (20-22°C). To maintain proper oxygenation of the tissue, a micromagnet agitated the solution during staining. After the staining, the tissue was washed in dye-free Tyrode's for 15 min and then moved to the perfusion chamber. The preparation was then constantly superperfused at 36.5±0.5°C. Two Ag/AgCl electrodes were immersed into the superfusion solution and placed on the sides of preparation to document pseudo-ECG. Imaging was conducted using 100 × 100 pixels MiCAM Ultima-L CMOS camera (SciMedia, USA Ltd., CA) from the endocardial fields of view ranging from 10 × 10 to 16 × 16 mm^2, sampled at 1,000 - 3,000 frames/sec. A 150-W halogen light system with built-in shutter (SciMedia) was used as an

excitation light source for the voltage dye. The filter set included a 520/44-nm excitation filter and 715 long-pass emission filter. The fluorescent signals were amplified, digitized, and visualized during the experiment using specialized software (SciMedia, USA Ltd., CA).

Data processing

A custom-made Matlab-based computer program was used to analyze optical APs offline.[7, 8] The signals were filtered using the low-pass Butterworth filter at 256 Hz. Activation times were measured directly from all optical APs using previously validated algorithms.[9] Membrane depolarization was defined as the time of maximum change in fluorescence (dF/dt_{max}) at each site and activation isochron maps were constructed. Conduction velocity was then calculated at different percentages of the PV preparation in the step of 10% under all conditions. Specifically, coordinates of fixed point on the PV_{ost} and of end point of PV_{dis} were recorded based on the *.bmp file of imaging field of view. Coordinates correlating to locations at different percentages of the preparation were then determined, which were also used to calculate the conduction velocity based on the activation map. A conduction velocity of zero was considered as the condition of conduction block.

For intra-PV conduction velocity measurements, we have used the relative PV distance to identify the location of conduction block within the PV. A starting point of the PV (0%) was defined as the pacing point, and the end of the PV (100%) was the physical end of the vein. Optical activation maps were reconstructed based on signals from each pixel within the PV. The conduction velocity was then measured at different relative PV distance. Therefore, conduction velocity of 0 did not necessarily occur at 100% of PV distance.

PV cell isolation and whole cell patch clamp electrophysiology

Patch clamp measurements of swelling-activated $I_{Cl,swell}$ current as well as spontaneous electrical activity were performed on cardiomyocytes separately isolated from PV distal and PV ostium, and on human induced pluripotent stem cell-derived cardiomyocytes (hiPSCs) generated from well-characterized DF19-9-11T line as described elsewhere.[10]

For PV cell isolation, the vein was isolated as abovementioned for *in vitro* preparations. After that, the vein was cut into three pieces: PV_{dis} as 1/3 of the distal part, and PV_{ost} as 1/3 of the ostium part,

separated by 1/3 of the middle part that was not used for cell isolation. PV_{dis} and PV_{ost} regions were then transferred, cut into small pieces and rinsed (4 min) in 'low Ca^{2+}/Mg^{2+}-free' solution containing (in mM): 140 NaCl, 5.4 KCl, 1.2 KH_2PO_4, 0.2 $CaCl_2$, 50 taurine, 18.5 glucose, 5 HEPES and 1 mg ml^{-1} bovine serum albumin, with pH adjusted to 6.9 with NaOH. PV tissue pieces were digested in 5 ml of 'low Ca^{2+}/Mg^{2+}-free' solution containing 1.84 mg/ml collagenase from Clostridium histolyticum (type V, Sigma-Aldrich, St. Louis, MO, USA) for 15 min. Then the tissue was transferred to 1ml of modified KB solution containing (in mM); 100 potassium glutamate, 10 potassium aspartate, 25 KCl, 10 KH_2PO_4, 2 $MgSO_4$, 20 taurine, 5 creatine, 0.5 EGTA, 20 glucose, 5 HEPES and 0.1% bovine serum albumin, with pH adjusted to 7.2 with KOH. The tissue was mechanically agitated using a wide bore pipette. This procedure yielded individual PV myocytes.

All patch-clamp experiments were carried out in the whole-cell configuration. Recordings on hiPSCs were performed at 36°C. Recordings on cardiomyocytes isolated from PV were performed at room temperature using the Axopatch 200B amplifier (Axon Instruments, Foster City, CA) with pCLAMP 10.7 software. Recording pipettes were pulled from thin walled borosilicate glass capillaries (World Precision Instruments, Inc., Sarasota FL) with pipette resistance of 3-5 MΩ. The recordings were filtered at 2 kHz and digitized at 20 kHz. For $I_{Cl,swell}$ measurements on hiPSCs, isosmotic 1T (T, relative osmolarity; isosmotic solution, 325 mOsm/kg H_2O) bath solution contained the following (in mM): 120 Mannitol, 80 NaCl, 5.4 KCl, 1 $MgCl_2$, 1.8 $CaCl_2$, 0.33 NaH_2PO_4, 10 HEPES, 10 glucose, 5 4-aminopyridine (4-AP), 0.2 $BaCl_2$, 0.2 $CdCl_2$, 1 µM atropine; pH = 7.4 (NaOH). Hypoosmotic (0.6T Tyrode) bath solution was made by removing mannitol from the isosmotic solution (205 mOsm/kg H_2O). 4-AP, $BaCl_2$, $CdCl_2$ and atropine were added to 1T and 0.6T Tyrode solutions to inhibit I_{to}/I_{kur}, I_{K1}, $I_{Ca,L}$ and $I_{K,ACh}$, respectively. The pipette solution for hiPSCs contained the following (in mM): 110 Cs-methansulfonate, 20 CsCl, 1 $MgCl_2$, 5 EGTA, 5 Na_2-phosphocreatine, 5 Mg-ATP, 0.1 Li-GTP, 10 HEPES; pH = 7.2 (CsOH). For hiPSCs whole-cell currents were recorded from a holding potential -40 mV with 300 ms test pulses from -110 to 30 mV, in 10 mV increments.

For action potential measurements, isosmotic 1T solution contained (mM): 120 Mannitol, 80 NaCl, 5.4 KCl, 1.8 $CaCl_2$, 1 $MgCl_2$, 10 HEPES and 10 Glucose; pH = 7.4 (NaOH), 320 mOsmol/L. Hypoosmotic bath solution 0.6T was made by removing mannitol from the isosmotic solution (200

mOsm/kg H_2O). Pipettes were filled with (mM): 140 KCl, 5 NaCl, 2 EGTA, 10 HEPES, 4 Mg-ATP; pH = 7.2 (KOH).

For $I_{Cl,swell}$ measurements on PV cells, isosmotic 1T (300 mOsm/kg H_2O) bath solution contained the following (in mM): 90 NMDG-Cl, 3 $MgCl_2$, 10 HEPES, 10 glucose, 5 CsCl, 0.5 $CdCl_2$, 91.9 Mannitol; pH = 7.4 (CsOH). Hypoosmotic (0.7T Tyrode) bath solution was made by removing mannitol from the isosmotic solution (208 mOsm/kg H_2O). The pipette solution for PV cells contained the following (in mM): 110 Cs-methansulfonate, 20 CsCl, 2.5 MgATP, 8 EGTA, 0.1 $CaCl_2$, 10 HEPES; pH = 7.1 (CsOH). For PV cells whole-cell currents were recorded from a holding potential -60 mV with 500 ms test pulses from -100 to 60 mV, in 10 mV increments.

Data were analyzed using Microcal Origin software (Origin Lab Corporation Northampton, MA USA).

Histology

To visualize PV structure, preparations were saved before and after stretch. The stretched PV preparations were fixed after optical mapping experiments performed with pathophysiological stretch (experimental series #5). To maintain the preparations stretched during fixation, at the end of the experiment the tissues were pinned to the thin silicon pad (at the same length as they were mapped) and then transferred to the fixation buffer. The preparations were fixed in 10% phosphate buffered formalin for 48 h and 70% ethanol for at least 24 h at 4°C, then paraffin embedded, sectioned along the PV and stained with Masson's trichrome (International Medical Equipment, San Marcos, CA, USA) [1, 11].

Immunohistochemistry

Immunofluorescence experiments were performed as previously described.[1, 11] In addition to histology, we used sister-sections for double-immunolabeling for caveolae scaffolding protein Caveolin-3 (1:300, mouse monoclonal, 610421, BD Biosciences, USA) or Caveolin-3 (1:300, rabbit polyclonal, ab2912, Abcam, USA) and volume-activated chloride channels ClC-2 (1:100, goat polyclonal, SAB2501373, Sigma, USA), ClC-3 (1:200, rabbit polyclonal, ACL-001, Alomone Labs, Israel), and SWELL1 (anti-LRRC8A, rabbit polyclonal, AAC-001, Alomone

Labs, Israel). For calculation of the sarcomere length before and after stretch, double-immunolabeling for α-actinin (1:600, mouse monoclonal, A5044, Sigma, USA) and Connexin-43 (1:800, rabbit polyclonal, C6219, Sigma, USA) were performed. Immunolabeling was carried out as described previously. Briefly, sections were dewaxed in xylene (10 min, twice), treated in ethanol (100%, 95%, and 79% for 5 min each), then washed in dH_2O for 5 min, treated with hydrogen peroxide (H_2O_2) in methanol for 30 min (1 ml of 30% H_2O_2 per 50 mL methanol), briefly washed in dH_2O, then treated with antigen unmasking solution (H-3300, Vector laboratories. Inc.) in microwave for 10 min (320 ml dH_2O + 3 ml antigen unmasking solution), then cooled at room temp for 30 min and finally washed in PBS (5 min, three times). Dewaxed sections were permeabilized with Triton X-100 (0.1%) for 10 min. After washing with PBS (two 10-min washes), sections were incubated with 1 ml blocking solution (2% BSA and 2% goat serum) for 2 h with gentle agitation at room temperature to block nonspecific binding. Subsequently, sections were incubated overnight with respective primary antibodies in blocking solution at 4°C. Excess primary antibody was washed off with the use of blocking solution (three 15-min washes). The sections were then incubated overnight with Alexa-conjugated secondary antibodies (Molecular Probes, Eugene, OR; 2 mg/ml) diluted 1:800 in blocking solution. The sections were then washed with blocking solution (three 30-min washes), resuspended in blocking solution, and mounted on a coverslip. To determine nonspecific binding, control experiments with secondary antibody alone were also performed.

Colocalization analysis

Colocalization plots were used to determine the amount of ClC-2, ClC-3 and SWELL1 that colocalized with Cav3 at different conditions. In a 2-channel confocal image, each voxel has two intensity values (ranging from 0 to 1 in a 12-bit image), one for each red and green staining. Voxels with intensities <0.3 were considered background fluorescence and were excluded from analysis. A colocalization plot, generated with a custom-made Matlab-based computer program, displays these intensity values as a function of each other. By definition, two proteins are highly colocalized in a particular volume when fluorescence intensities corresponding to these two proteins are high in the voxel corresponding to this volume (*1, 3*). Therefore, if two proteins are colocalized in many voxels, the colocalization plot will contain a significant diagonal distribution. Voxels with the highest degree of colocalization will be displayed in the upper right quadrant. In contrast, if the

two proteins are not colocalized, the colocalization plot shows voxel values near each axis, with no diagonal elements present.

Quantitative real-time polymerase chane reaction (qRT-PCR) analysis

Total RNA was extracted from rat PV distal, PV ostium and LAA as previously described.[12] Briefly, tissue was homogenized in TriZol reagent (Invitrogen) according to the manufacturer's instruction. Total RNA was treated with DNaseI (RNase-free DNase set; Qiagen) for one hour and purified using the RNeasy® miniElute kit (Qiagen). First strand cDNA synthesis was performed using the iScript™ Reverse Transcription Kit (Biorad). Specifically, samples were incubated at 50ºC for 90 minutes prior to heat inactivation of the reverse transcriptase at 70ºC for 15 minutes, oligo dT priming and 200 to 500 ng of total RNA as template. mRNA levels of *ClC-2, ClC-3, LRRC8A* (for SWELL1 channels), *ANO1* (or TMEM16A, Ca^{2+}-activated chloride channels) *Cav3* and *GAPDH* (responsible for house-keeping gene) were assessed using TaqMan® gene expression assays. Detailed primer information is described in **Table S1**. The equivalent of 10 ng reverse transcribed RNA and TaqMan™ Fast Advanced Master Mix (Thermo Fischer Scientific™) was used in the TaqMan® qPCR reactions. Thermal cycling and fluorescence measurement was performed in an MXPro5000 Real-Time PCR System (Stratagene). Data was analyzed using MXPro5000 software (Stratagene). mRNA levels were quantified using the ΔΔCT-method and normalized to GAPDH housekeeping gene.

Immunoprecipitation

For immunoprecipitations, rat PV or healthy human LA tissue lysates were used, and immunoprecipitations were carried out using anti-Cav-3, ClC-2, ClC-3, SWELL1 and respective control IgG antibodies were used at the same concentrations. Immune complexes were analyzed by Western blot□ClC-2, ClC-3, Cav3, and GAPDH. Briefly, tissue samples from rat and human were flash frozen in liquid nitrogen, homogenized and lysed using buffer containing 150 mM NaCl, 25 mM Tris·HCl, 10 mM NaEGTA, 20 mM NaEDTA, and supplemented with 0.5% CHAPS and 1x protease inhibitor cocktail (B14001, bimake). The lysate (500 μg) was sonicated, rotated at 4ºC for 2 hours and centrifuged at 16,000 × g for 15 min at 4ºC. The soluble supernatant was incubated with aforementioned antibodies (20 μg) at 4ºC for 2 hours and then incubated with 25 μL (Protein A Mag Sepharose/Protein G Mag Sepharose, 28944006 /28944008, GE Life

Sciences; 1:1 Protein A/G) at 4ºC for 2 hours, followed by incubation with anti-Cav-3 (rabbit polyclonal, ab2912, Abcam, USA), anti-ClC-2 (goat polyclonal, SAB2501373, Sigma, USA), anti-ClC-3 (rabbit polyclonal, ACL-001, Alomone Labs, Israel), anti-SWELL1 (rabbit polyclonal, AAC-001, Alomone Labs, Israel) or control rat IgG (sc-2026, Santa Cruz Biotechnology, USA) in a total of 300-400 μL (depending on protein concentration) of lysate. After flowthrough collection, samples were eluted with 2.5% Acetic Acid. Laemmli Buffer (161-0747, Bio-Rad) and DTT were added and all samples were incubated at 65ºC for 10 min. Immune complexes were analyzed by SDS-PAGE (4-20% gradient gels, Bio-Rad) and Western blot by probing with antibodies to Cav3, ClC-2, ClC-3, SWELL1, and GAPDH (mouse monoclonal, MAB374, Millipore).

Transmission Electron Microscopy

Rapidly excised rat hearts were initially perfused with ice cold Tyrode's solution in a Langendorff perfusion system, then samples of interest were isolated and fixed in the following fixative: 2.5% glutaraldehyde, 2.0% paraformaldehyde, and 0.2 mol/liter cacodylate buffer for 24-48 hours. The samples were rinsed in the same buffer, postfixed in 1% osmium tetroxide, dehydrated in a graded ethanol series, rinsed in propylene oxide, and embedded in Epon 812 substitute. After resin polymerization, the samples were then sliced into 70-nm sections with a Leica EM UC6 ultramicrotome and placed on 200 mesh transmission electron microscopy grids. The samples were post-stained in 8% uranyl acetate in 50% EtOH and Reynold's lead citrate, viewed on a Philips CM120 transmission electron microscope, and documented with a SIS MegaView III digital camera. Electron microscopy images were analyzed by using the NIH ImageJ software. A threshold size for individual caveolae was set between 40 and 100 nm. The number of caveolae was counted as per unit length (μm) of myocyte sarcolemmal membranes from a series of random electron microscopy micrographs.

Chemicals

All chemicals were obtained from Sigma-Aldrich (St. Louis, MO, USA) unless noted otherwise. Chloride channels inhibitors (DIDS, 9AC, DCPIB, NPPB) were obtained from Tocris Bioscience (Bristol, UK).

Statistics

Student *t* test was used in two-group comparisons. Multiple groups of normally distributed data of similar variance were compared by one- or two-way ANOVA. For multiple comparisons, the Bonferroni's corrected P value is shown. Categorical variables were compared by $\chi 2$ test. All statistical analyses were performed using GraphPad Prism 5 or Origin version 6.1. A value of $P < 0.05$ was considered statistically significant. Values were presented as mean ± SEM.

Table S1. List of Taqman® probes for RT-qPCR analysis of sarcolemmal chloride channel isofors and caveolar scaffolding protein Caveolin-3 mRNA expression in rat hearts.

Rat:	Caveolin-3	Rn00755343_m1
	ClC-2	Rn00567553_m1
	ClC-3	Rn01535195_m1
	SWELL1 (LRRC8A)	Rn01436310_m1
	ANO1 (TMEM16A)	Rn01474520_m1

Figure S1. Effect of physiological stretch on PV electrical activity.

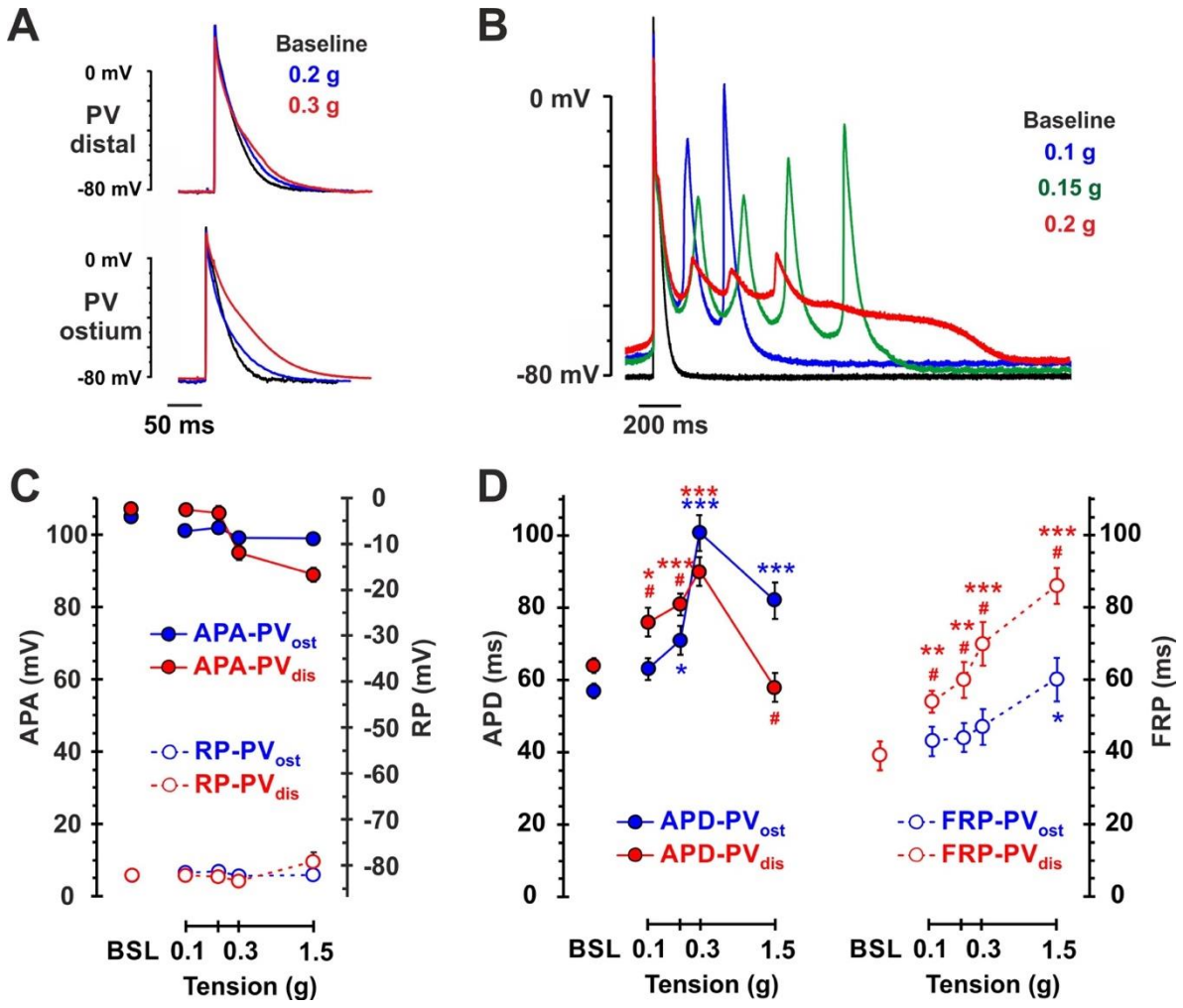

(**A**) Action potentials (APs) were simultaneously recorded from PV_{ost} (*bottom recordings*) and PV_{dis} (*upper recordings*) under progressive application of 0.1, 0.2, 0.3, and 1.5 g tensions. (**B**) Superimposed recording of spontaneous APs from the PV, with early after depolarizations observed at different tensions. Presence of spontaneous activity was measured when electrical stimulation was stopped. (**C**) AP amplitude (APA) and membrane resting potential (RP) changes in PV_{ost} and PV_{dis} under stretch. (**D**) AP duration at 90% of repolarization (APD) and functional refractory period (FRP) measured at different tensions. n=8 WT rats. *, **, *** – $P<0.05$, <0.01, <0.001 within the same group vs. baseline (BSL). $^{\#, \#\#, \#\#\#}$ – $P<0.05$, <0.01, <0.001 for PV_{dis} vs. PV_{ost} by two-way ANOVA with Bonferroni correction.

Figure S2. (**A**) Representative APD restitution curves are shown for PV_{dis} and PV_{ost} at baseline and at 0.3 g tension. (**B**) Change of APD restitution curve slopes for PV_{dis} and PV_{ost} at physiological stretch protocol (0 – 1.5 g).

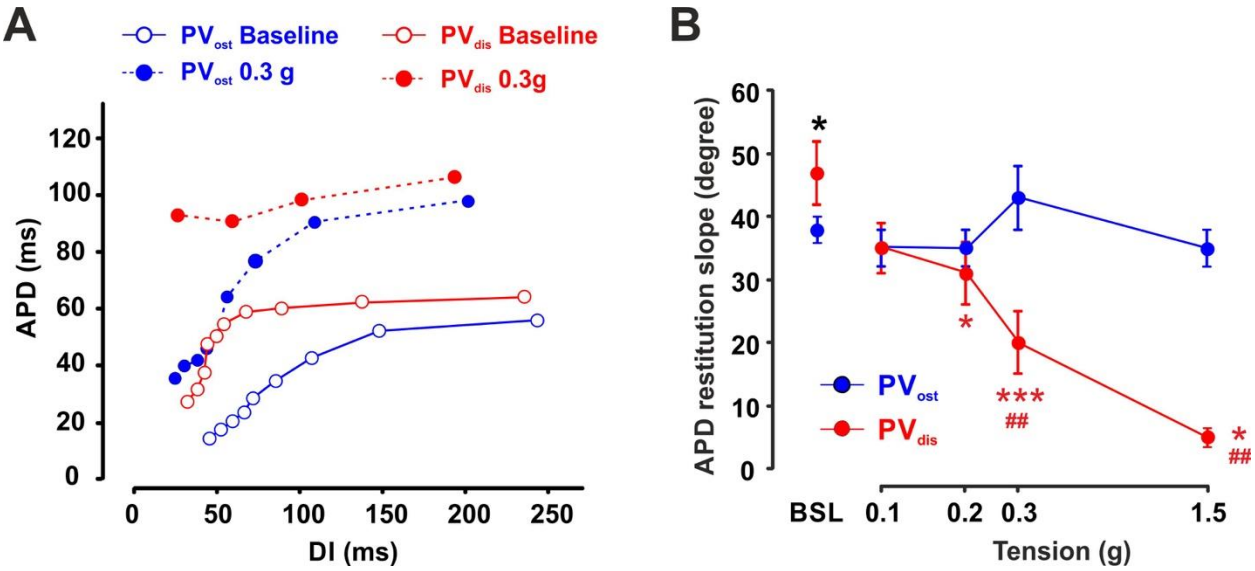

*** – <0.001 within the same group vs. baseline (BSL). ## –<0.01 for PV_{dis} vs. PV_{ost}.

Figure S3. Effect of pathophysiological stretch on the PV myocardium action potential duration at 90% of repolarization (APD, **A**) and functional refractory period (FRP, **B**).

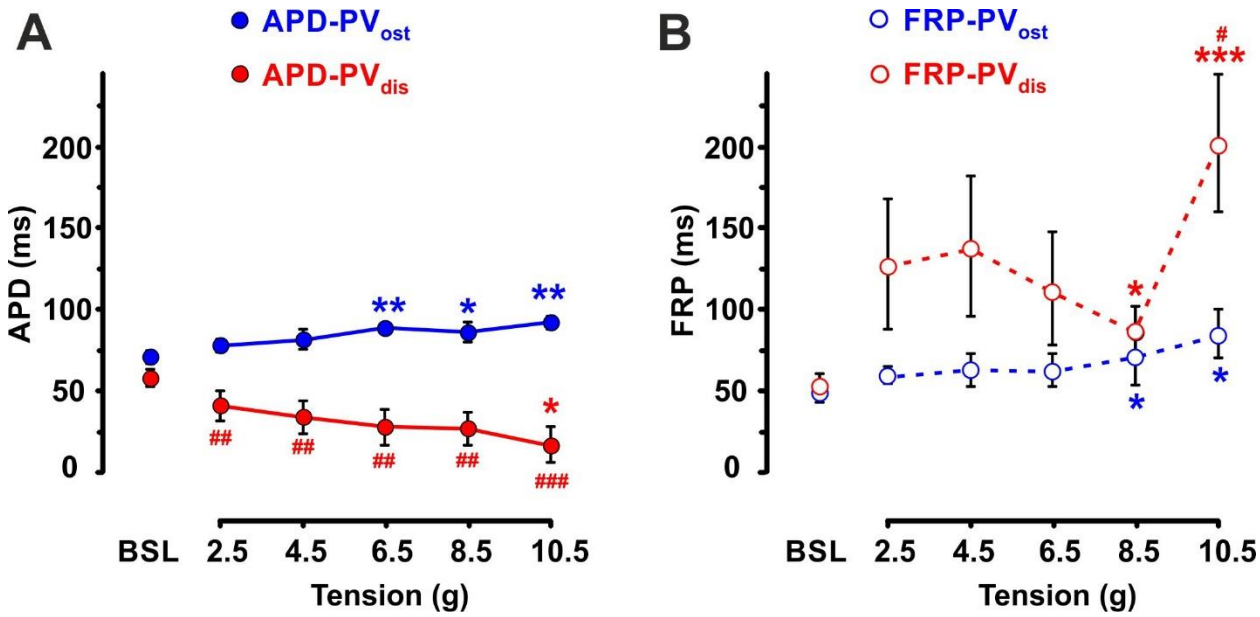

A loss of rate-dependent APD adaptation was observed in PV_{dis} where APD restitution curve slope became flattened (from 47±5 at baseline to 4±1 at 10.5 g, $P<0.001$), whereas APD restitution curve remained steep in PV_{ost} (38±2 at baseline vs. 24±5 at 10.5 g, *NS*).

Figure S4. Sarcomere length measured from immunofluorescent staining against α-actinin staining as an average distance between α-actinin striated bands within cells in PV_{dis} and PV_{ost} at baseline (no stretch applied) and under pathological stretch (at tensions required to induce intra-PV conduction block).

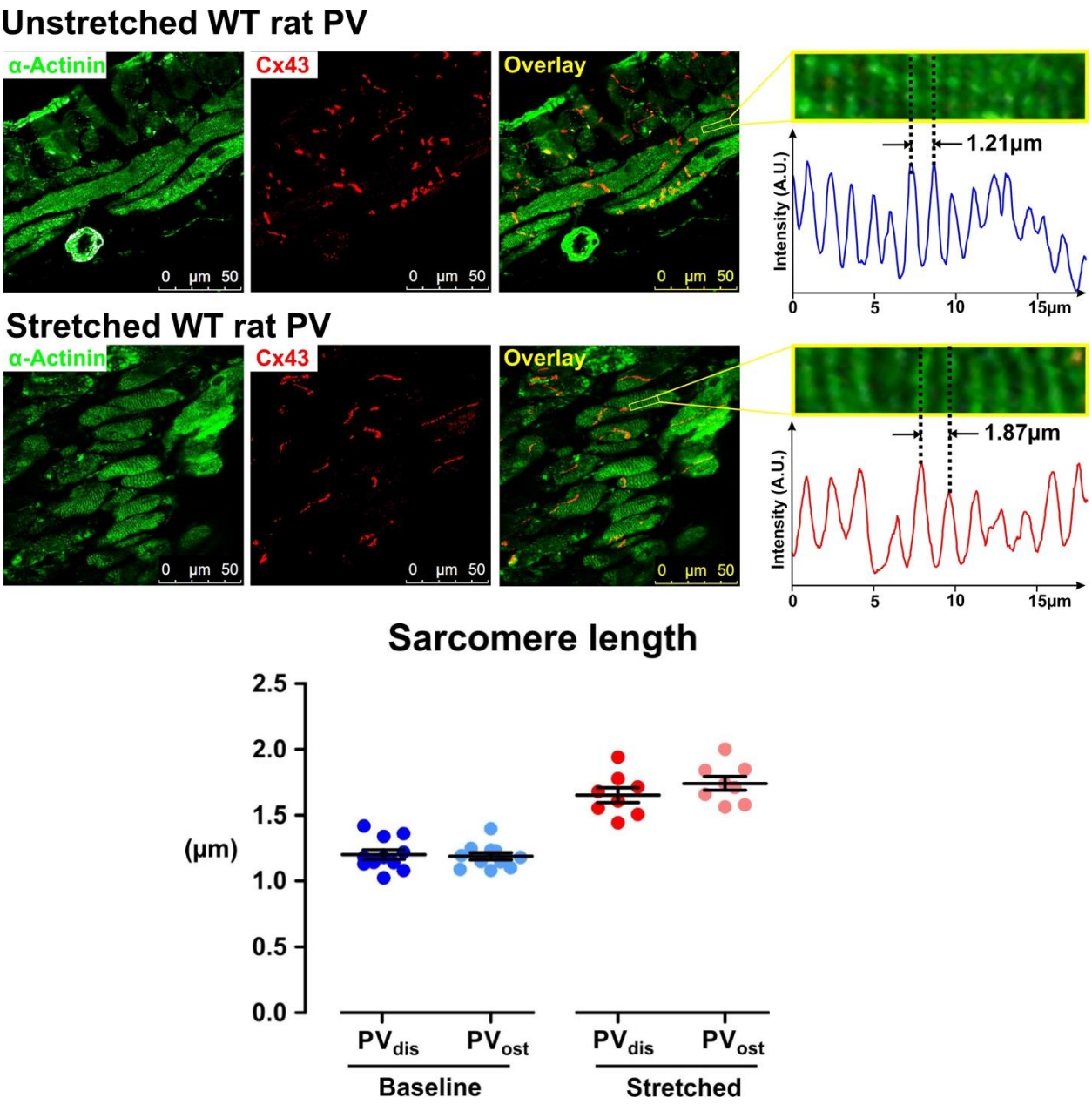

Figure S5. Combined effect of stretch and norepinephrine (NE, 1 µM) superfusion on spontaneous electrical activity of the pulmonary vein (PV).

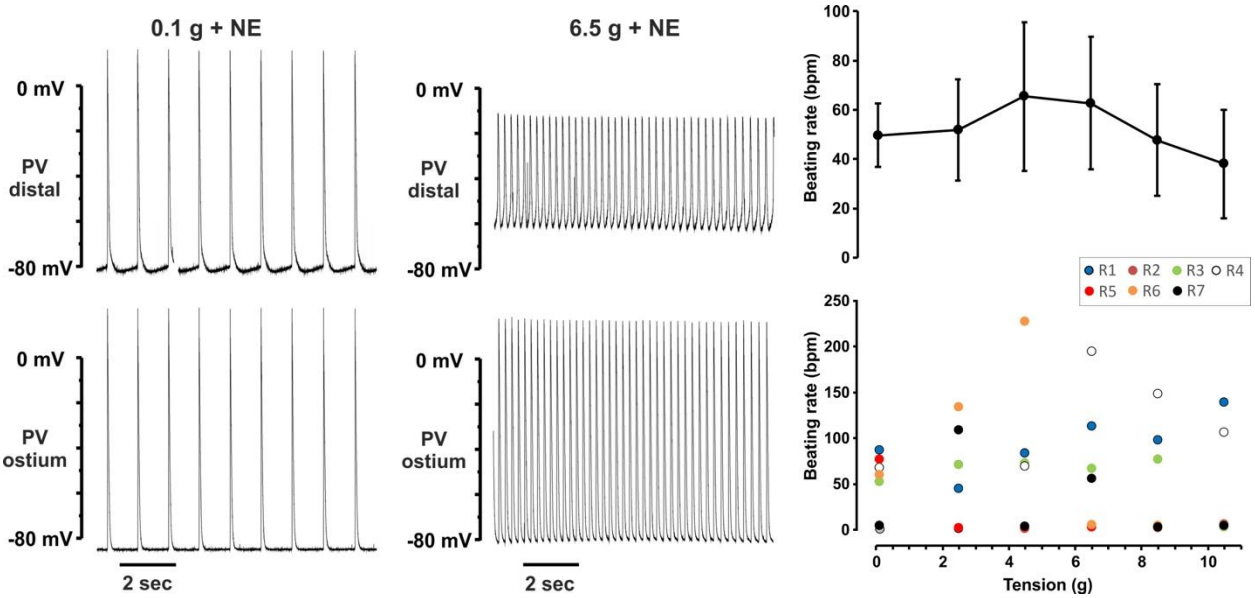

Representative examples of norepinephrine superfusion on spontaneous electrical activity of the PVs at physiological (0.1 g, *left*) and pathophysiological (6.5 g, *middle*) tensions applied. Action potentials were simultaneously recorded from the distal part of the PV (top recordings) and the PV ostium (bottom recordings). At pathological stretch, due to depolarized resting potential, NE more frequently resulted in continuous stable spontaneous activity in PV_{dis} (note resting potential depolarization at 6.5 g tension). *Right*: Average spontaneous beating rate (*upper panel*, n=8) and individual rat beating rates (*lower panel*) recorded at different tensions after application of NE. Note that different rats have maximal beating rate at different tensions; an average tension where rats had the highest beating rate under NE application, was 6.2 ± 1.5 g.

Figure S6. Micro-reentry within the pulmonary vein (PV).

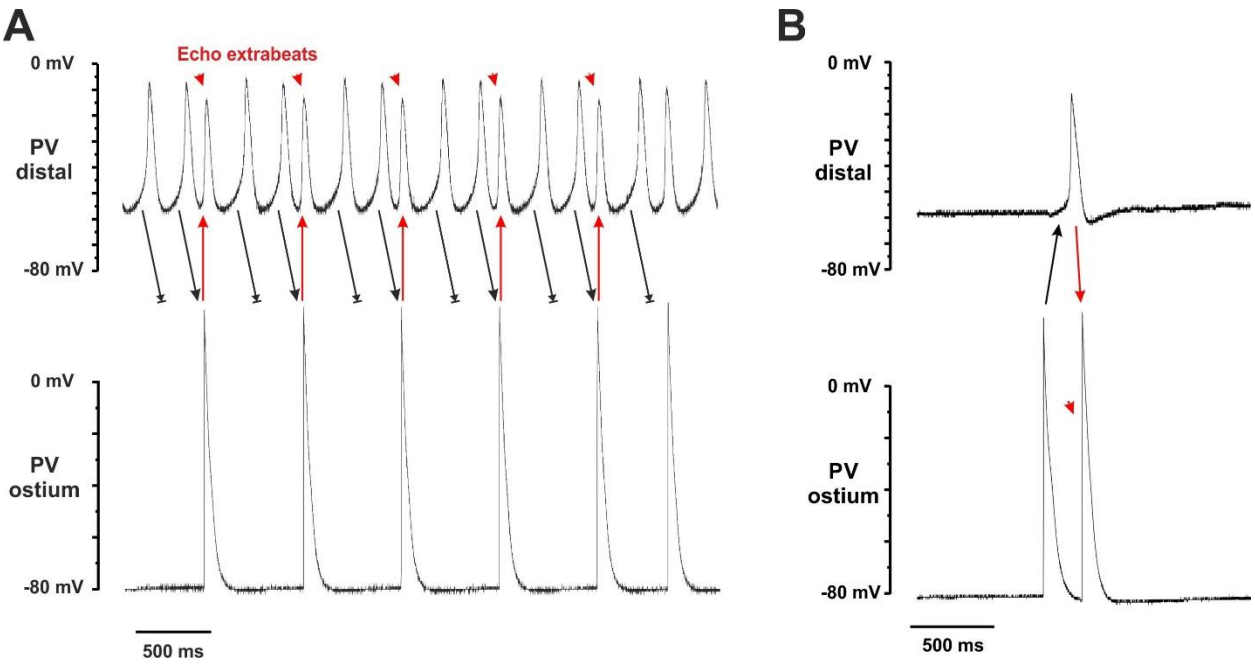

Action potentials were simultaneously recorded from the distal part of the PV (top recordings) and the PV ostium (bottom recordings). (**A**) Alterations between non-propagating spontaneous beats and beats which propagated into PV ostium and then re-excited PV distal (shown by a dotted line) inducing premature action potentials (echo extrabeats, labelled by arrows). (**B**) Single extra-beat induced by spontaneous excitation of PV ostium which reflected from the PV distal and then re-excited PV ostium (shown by red arrow).

Figure S7. Negative control for immunofluorescent staning experiments.

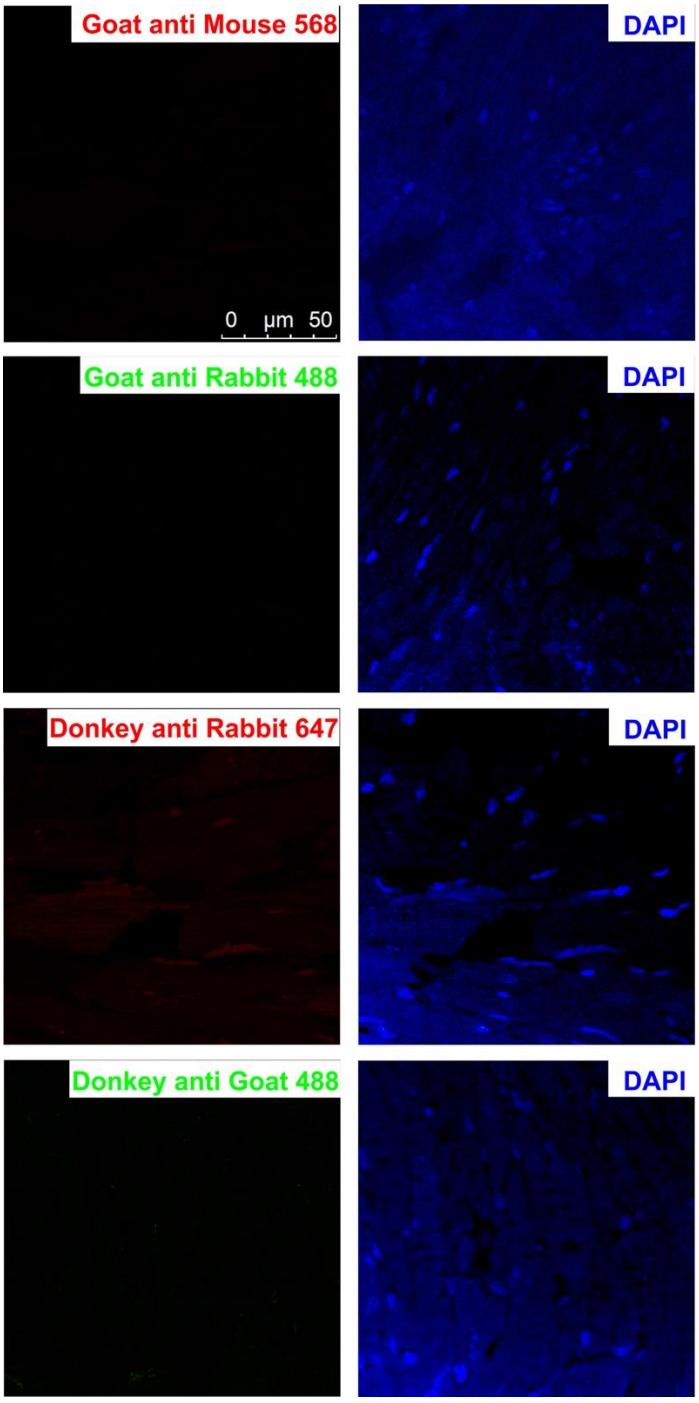

Figure S8. Co-IP Western Blots, from left to right: inputs, immune complexes, supernatants, and Laemmli/DTT elution.

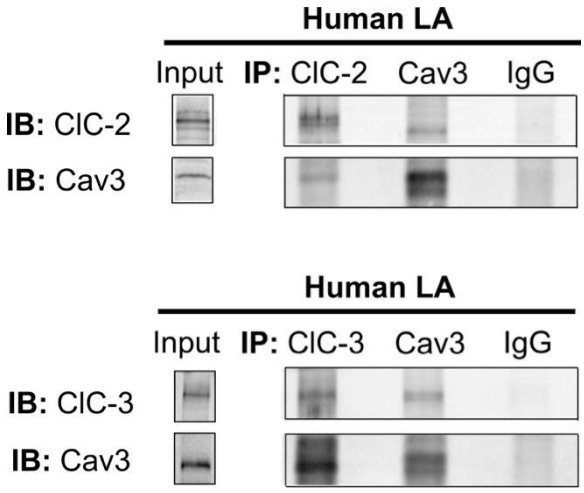

Cav3 and ClC-2 (*top*) and Cav3 and ClC-3 (*bottom*) in human LA myocardium lysate. n=2.

Figure S9. Echocardiography data for 9-12 months old WT (n=5) and SHR (n=3) rats.

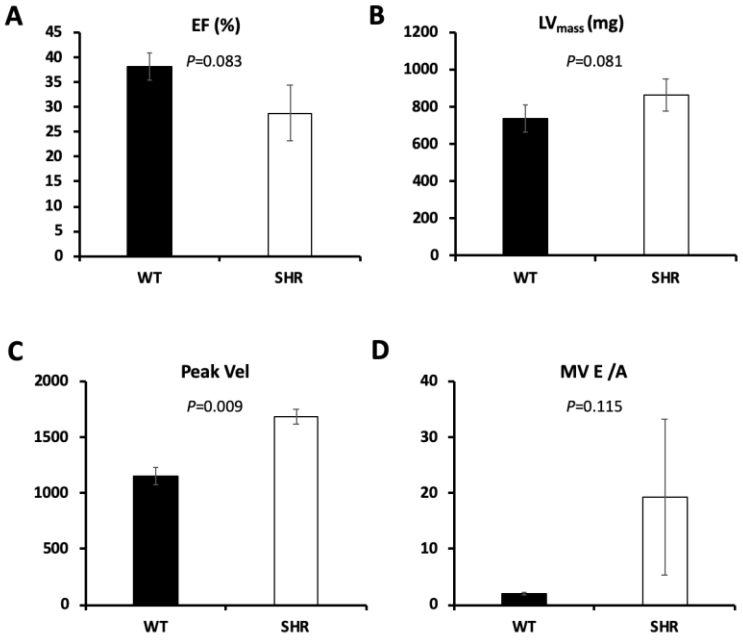

Ejection fraction (EF, A), corrected left ventricle mass (LV_{mass}, B), peak velocity (C) and MV E/A (D) are shown. ** – $P<0.01$ vs. baseline by unpaired Student *t* test.

Figure S10. SHR PV electrophysiological characteristics at baseline.

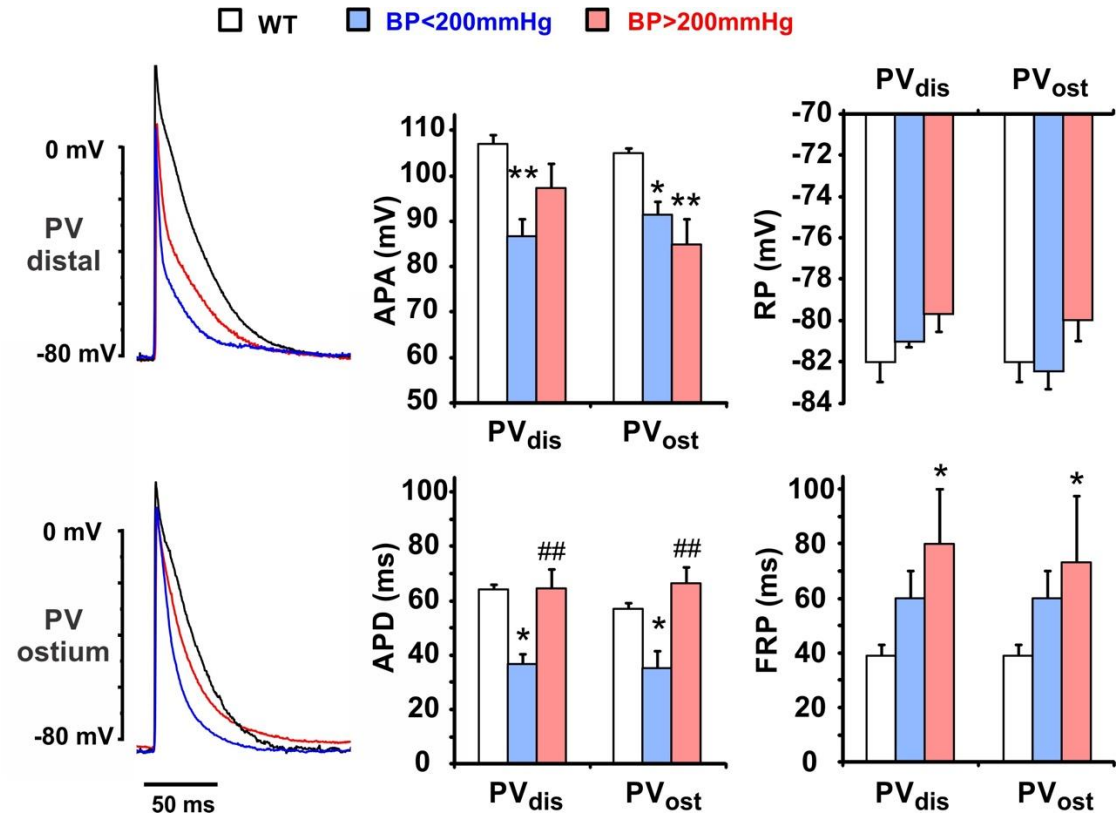

Left: representative APs for WT rats (*black*) and SHRs with BP of <200 mm Hg (*blue*) and >200 mm Hg (*red*) at baseline are shown superimposed for PV_{dis} and PV_{ost}. *Right*: AP parameters are shown for three groups of rats at baseline. *, ** – P<0.05, <0.01 vs. WT; $^{\#\#}$ – P<0.01 vs. SHRs with BP<200 mmHg by one-way ANOVA with Bonferroni correction.

Supplemental References:

1. Glukhov AV, Fedorov VV, Kalish PW, Ravikumar VK, Lou Q, Janks D, Schuessler RB, Moazami N and Efimov IR. Conduction remodeling in human end-stage nonischemic left ventricular cardiomyopathy. *Circulation*. 2012;125:1835-47.

2. Lou Q, Fedorov VV, Glukhov AV, Moazami N, Fast VG and Efimov IR. Transmural heterogeneity and remodeling of ventricular excitation-contraction coupling in human heart failure. *Circulation*. 2011;123:1881-90.

3. Glukhov AV, Fedorov VV, Lou Q, Ravikumar VK, Kalish PW, Schuessler RB, Moazami N and Efimov IR. Transmural dispersion of repolarization in failing and nonfailing human ventricle. *Circ Res*. 2010;106:981-91.

4. Cheng TC, Philip JL, Tabima DM, Hacker TA and Chesler NC. Multiscale structure-function relationships in right ventricular failure due to pressure overload. *Am J Physiol Heart Circ Physiol*. 2018;315:H699-H708.

5. Egorov YV, Kuz'min VS, Glukhov AV and Rosenshtraukh LV. Electrophysiological Characteristics, Rhythm, Disturbances and Conduction Discontinuities Under Autonomic Stimulation in the Rat Pulmonary Vein Myocardium. *J Cardiovasc Electrophysiol*. 2015;26:1130-9.

6. Egorov YV, Glukhov AV, Efimov IR and Rosenshtraukh LV. Hypothermia-induced spatially discordant action potential duration alternans and arrhythmogenesis in nonhibernating versus hibernating mammals. *Am J Physiol Heart Circ Physiol*. 2012;303:H1035-46.

7. Lang D and Glukhov AV. High-resolution Optical Mapping of the Mouse Sino-atrial Node. *Journal of visualized experiments : JoVE*. 2016.

8. Lou Q, Hansen BJ, Fedorenko O, Csepe TA, Kalyanasundaram A, Li N, Hage LT, Glukhov AV, Billman GE, Weiss R, Mohler PJ, Gyorke S, Biesiadecki BJ, Carnes CA and Fedorov VV. Upregulation of adenosine A1 receptors facilitates sinoatrial node dysfunction in chronic canine heart failure by exacerbating nodal conduction abnormalities revealed by novel dual-sided intramural optical mapping. *Circulation*. 2014;130:315-24.

9. Fedorov VV, Kostecki G, Hemphill M and Efimov IR. Atria are more susceptible to electroporation than ventricles: implications for atrial stunning, shock-induced arrhythmia and defibrillation failure. *Heart Rhythm*. 2008;5:593-604.

10. Lian X, Hsiao C, Wilson G, Zhu K, Hazeltine LB, Azarin SM, Raval KK, Zhang J, Kamp TJ and Palecek SP. Robust cardiomyocyte differentiation from human pluripotent stem cells via temporal modulation of canonical Wnt signaling. *Proceedings of the National Academy of Sciences of the United States of America*. 2012;109:E1848-57.

11. Glukhov AV, Kalyanasundaram A, Lou Q, Hage LT, Hansen BJ, Belevych AE, Mohler PJ, Knollmann BC, Periasamy M, Gyorke S and Fedorov VV. Calsequestrin 2 deletion causes sinoatrial node dysfunction and atrial arrhythmias associated with altered sarcoplasmic reticulum calcium cycling and degenerative fibrosis within the mouse atrial pacemaker complex1. *European heart journal*. 2015;36:686-97.

12. de Lange WJ, Hegge LF, Grimes AC, Tong CW, Brost TM, Moss RL and Ralphe JC. Neonatal mouse-derived engineered cardiac tissue: a novel model system for studying genetic heart disease. *Circ Res*. 2011;109:8-19.